nature communications

Article

https://doi.org/10.1038/s41467-024-51956-9

Feedforward inhibition of stress by brainstem neuropeptide Y neurons

Received: 17 January 2024

Accepted: 20 August 2024

Published online: 01 September 2024

Check for updates

Yan Zhang[1,2,3,13], Jiayi Shen[4,13], Famin Xie[1], Zhiwei Liu[4], Fangfang Yin[5], Mingxiu Cheng[6,7], Liang Wang[4], Meiting Cai[3], Herbert Herzog[8,9], Ping Wu[5], Zhi Zhang[1] ✉, Cheng Zhan[3,4] ✉ & Tiemin Liu[1,2,10,11,12] ✉

Resistance to stress is a key determinant for mammalian functioning. While many studies have revealed neural circuits and substrates responsible for initiating and mediating stress responses, little is known about how the brain resists to stress and prevents overreactions. Here, we identified a previously uncharacterized neuropeptide Y (NPY) neuronal population in the dorsal raphe nucleus and ventrolateral periaqueductal gray region (DRN/vlPAG) with anxiolytic effects in male mice. $NPY^{DRN/vlPAG}$ neurons are rapidly activated by various stressful stimuli. Inhibiting these neurons exacerbated hypophagic and anxiety responses during stress, while activation significantly ameliorates acute stress-induced hypophagia and anxiety levels and transmits positive valence. Furthermore, $NPY^{DRN/vlPAG}$ neurons exert differential but synergic anxiolytic effects via inhibitory projections to the paraventricular thalamic nucleus (PVT) and the lateral hypothalamic area (LH). Together, our findings reveal a feedforward inhibition neural mechanism underlying stress resistance and suggest $NPY^{DRN/vlPAG}$ neurons as a potential therapeutic target for stress-related disorders.

Stress affects the physiological functions and behaviors of individuals, yielding both positive and negative outcomes. On the positive side, stressors trigger the fight and flight response that is crucial to the performance and survival under threats[1]. On the negative side, impaired adaptation and resistance to stressful events can precipitate the onset or relapse of symptoms in a range of psychiatric and behavioral disorders, including anxiety[2], depression[3], hyperphagia[4] or hypophagia[5], and even posttraumatic stress disorder (PTSD)[6]. A balance between two opposing stress and anti-stress mechanisms determines the overall impact of stress. The former renders organisms more sensitive and vulnerable to stress-related disorders, while the later imparts resilience and resistance. Thus, identifying mechanisms that make individuals resistant or less vulnerable to stressful stimuli is an important approach for the prevention of stress-related disorders. Recent studies showed that many brain areas (such as the amygdala[4], hypothalamus[7] and hippocampus[8]) are implicated in initiating or mediating stress-induced changes in emotion and behavior. However, relatively little is known about the neuronal mechanisms of anti-stress, especially at the neural circuit level.

Neuropeptide Y (NPY) is a 36-amino-acid peptide that plays important roles in the control of many basic physiological functions and behaviors, including vasoconstriction[9], energy metabolism[10], and

[1]State Key Laboratory of Genetic Engineering, School of Life Sciences, Fudan University, Shanghai, China. [2]Human Phenome Institute, Fudan University, Shanghai, China. [3]Hefei National Research center for Physical Sciences at the Microscale, University of Science and Technology of China, Hefei, China. [4]Center for Advanced Interdisciplinary Science and Biomedicine of IHM, Division of Life Sciences and Medicine, University of Science and Technology of China, Hefei, China. [5]Institute of Artificial Intelligence, Hefei Comprehensive National Science Center, Hefei, China. [6]National Institute of Biological Sciences, Beijing, China. [7]Tsinghua Institute of Multidisciplinary Biomedical Research, Tsinghua University, Beijing, China. [8]St Vincent's Centre for Applied Medical Research, Faculty of Medicine, UNSW, Sydney, NSW, Australia. [9]Faculty of Medicine, University of New South Wales, Sydney, NSW, Australia. [10]Shanghai Key Laboratory of Metabolic Remodeling and Health, Institute of Metabolism & Integrative Biology, Fudan University, Shanghai, China. [11]Department of Endocrinology and Metabolism, Zhongshan Hospital, Shanghai, China. [12]School of Life Sciences, Inner Mongolia University, Hohhot, China. [13]These authors contributed equally: Yan Zhang, Jiayi Shen. ✉e-mail: z_zhang@fudan.edu.cn; zhancheng@ustc.edu.cn; tiemin_liu@fudan.edu.cn

feeding behavior[11]. In addition, a number of reports indicate that NPY has anti-stress properties[12]. Direct administration of NPY into the brain ventricle or multiple brain areas reduces anxiety[13,14], and high cerebral levels of NPY can prevent the development of stress-induced behavior disruption and freezing[15]. Consistently, NPY knockout mice are more anxious[16], and individuals with lower cerebral levels of NPY are more vulnerable to trauma-induced diseases such as PTSD[17]. Given the potent anxiolytic effects of NPY, it was recently under investigation in clinical trials[18] (NCT01533519) as a therapeutic option for managing stress-related psychiatric disorders. NPY neurons are widely distributed throughout the brain[19], including the cortex, hypothalamus, thalamus, hippocampus, and brainstem. However, which population of NPY neurons exerts anxiolytic effects, whether they are stressor-specific and how they interact with stress-related circuits remain unknown.

In the present study, employing a combination of immediate early gene activation and in vivo fiber photometry recording of neuronal activity, we successfully identify a population of brainstem NPY neurons that responds quickly and strongly to various stress stimuli. Manipulating these NPY neurons using chemogenetic and optogenetic approaches ameliorate acute stress-induced hypophagia and anxiety levels through inhibitory neural circuits. Our study provides mechanistic insights into how the brain actively resists stress and help with the development of novel therapeutic strategies for stress-related disorders.

Results

$NPY^{DRN/vlPAG}$ neurons are activated by acute novelty stress

To search for anxiolytic NPY neurons, we adopted an acute novelty stress paradigm[20], in which group-housed mice were individually transferred into new empty cages without padding materials (Fig. 1a) for 24 hs. Novelty stress significantly suppressed feeding in the first 4 hs (Fig. 1b), followed by a food intake increase during 4-24 hs (Fig. 1c), which may represent a compensatory effect aimed at restoring homeostasis in the body. Despite a slightly increase, the total 24-h food intake during the whole stress period was not significantly altered (Fig. 1c). Based on this observation, the food intake over a 24-h period during novelty stress was measured in the following experiment, as 24 hs is sufficiently to capture the entire dynamic process of feeding inhibition and subsequent recovery. Moreover, 1-h novelty stress significantly increased serum levels of corticosterone (Fig. 1d), a prevalent marker for stress level. Elevated plus maze (EPM) and open field test (OFT) are common anxiety-assessment behavior tests, in which anxiety level inversely correlates with the time animals spend in the open arms and the time that animals explored the center of the arena, respectively. We examined how acute novelty stress influences behaviors in EPM and OFT (Supplementary Fig. 1a). 2-h novelty stress significantly decreased time mice spent on the open arm of the EPM (Fig. 1e, f), as well as time spent and distance traveled in the center of the OFT (Fig. 1g, h). Of note, total distance in the open field test didn't differ between groups (Fig. 1h), meaning that novelty stress didn't influence locomotor activity. Collectively, these results suggested that novelty stress induces acute hypophagia and increases stress levels.

We then performed whole-brain Fos immunostaining to identify neurons activated by acute novelty stress. After 2-h novelty stress, mice were sacrificed and whole-brain Fos expression was visualized by immunofluorescence. Consistent with previous reports, we observed significantly increased Fos signaling in multiple stress-related brain regions, such as the medial preoptic area/medial preoptic nucleus (MPA/MPO)[21], paraventricular thalamic nucleus (PVT)[22], paraventricular hypothalamic nucleus (PVN)[23], and basolateral amygdaloid nucleus (BLA)[24] (Supplementary Fig. 1b, c). In addition, there were significantly more Fos^+ neurons in the dorsal raphe nucleus and ventrolateral periaqueductal gray region (DRN/vlPAG) of stress-exposed mice than in control mice (Supplementary Fig. 1b, c). Notably, a considerable proportion of Fos^+ neurons in the DRN/vlPAG region are NPY neurons (Fig. 1i, j), suggesting that $NPY^{DRN/vlPAG}$ neurons were activated by acute novelty stress.

To further uncover the dynamic activity of $NPY^{DRN/vlPAG}$ neurons in response to stress, we performed fiber photometry recording of $NPY^{DRN/vlPAG}$ neuronal calcium signals in freely behaving mice (Fig. 1k). GCaMP6m adeno-associated virus (AAV) was injected into the DRN/vlPAG region of $Npy^{ires\text{-}Cre}$ mice to express GCaMP6m in $NPY^{DRN/vlPAG}$ neurons (Supplementary Fig. 2a). AAV-DIO-mGFP was injected as a negative control. In the novelty stress test, we observed a transient increase in $NPY^{DRN/vlPAG}$ neuronal activity when mice were transferred from home cages to new empty cages. $NPY^{DRN/vlPAG}$ neurons showed significantly higher neuronal activity when the mice were in new cages compared to their activity in home cages (Fig. 1l). This increased activity gradually decreased to baseline level in several minutes (Supplementary Fig. 2b). We next extended the novelty stress to 4 hs and recorded $NPY^{DRN/vlPAG}$ neuronal activity before, during and after chronic novelty stress. Similar to the results above, there was no significant changes of $NPY^{DRN/vlPAG}$ neurons during or after long-term novelty stress (Supplementary Fig. 2c). Taken together, these data indicate that $NPY^{DRN/vlPAG}$ neurons respond quickly and strongly to the onset of acute novelty stress.

$NPY^{DRN/vlPAG}$ neurons respond to various stressful stimuli

To assess whether $NPY^{DRN/vlPAG}$ neurons respond specifically to particular stress or various stress types, we employed behavioral models beyond acute novelty stress. In the tail-suspension test, $NPY^{DRN/vlPAG}$ neuronal activity underwent a rapid and robust increase and quickly returned to baseline when mice were returned back to their home cages (Supplementary Fig. 2d). Interestingly, we observed an increase in fluorescence caused by the approaching of the experimenter to the mice even before applying stress, suggesting that $NPY^{DRN/vlPAG}$ neurons are highly sensitive to stress. Similarly, $NPY^{DRN/vlPAG}$ neuronal activity increased when mice approached and interacted with a novel object (Supplementary Fig. 2e). Grooming, a typical compulsive behavior associated with stress or neuropsychological diseases[25] did not elicit any changes of $NPY^{DRN/vlPAG}$ neuronal activity (Supplementary Fig. 2f), which needs further investigations. Standing up in the cage is a sign of exploration. $NPY^{DRN/vlPAG}$ neuronal activity increased when the mice stood up (Supplementary Fig. 2g), with no difference in calcium signal magnitude between novel cage and home cage (Supplementary Fig. 2h).

Apart from stress, we also examined calcium dynamics regarding feeding behavior. After an overnight fasting, $NPY^{DRN/vlPAG}$ neurons exhibited reduced neuronal activity when the mice ate chow diet (Supplementary Fig. 2i). Together, these findings indicate that stress-related behaviors increase whereas food consumption suppresses $NPY^{DRN/vlPAG}$ neuronal activity, highlighting the pivotal role of $NPY^{DRN/vlPAG}$ neurons in coping stress-induced feeding.

$NPY^{DRN/vlPAG}$ neurons are essential and sufficient for resisting novelty stress-induced hypophagia

To determine the role of $NPY^{DRN/vlPAG}$ neurons in regulating the stress response, we used chemogenetic approaches to selectively manipulate these neurons[26]. To inhibit $NPY^{DRN/vlPAG}$ neurons, a Cre-dependent inhibitory chemogenetic vector, AAV-DIO-hM4Di-eGFP, was injected into the DRN/vlPAG region of $Npy^{ires\text{-}Cre}$ mice (referred to as NPY^{hM4Di} mice). In vitro electrophysiological recordings confirmed that clozapine N-oxide (CNO), a ligand of hM3Dq and hM4Di, successfully inhibited NPY^{hM4Di} neurons by decreasing neuronal membrane potential and firing frequency (Fig. 2a and Supplementary Fig. 3a). Fluorescence in situ hybridization (FISH) results showed that the majority (~95%, 388 neurons from 3 brain slices) of $hM4Di^+$ neurons co-expressed *Npy* (Fig. 2b). CNO (2 mg/kg) was intraperitoneal (i.p.) injected into NPY^{hM4Di} mice half an hour prior to novelty

https://doi.org/10.1038/s41467-024-51956-9

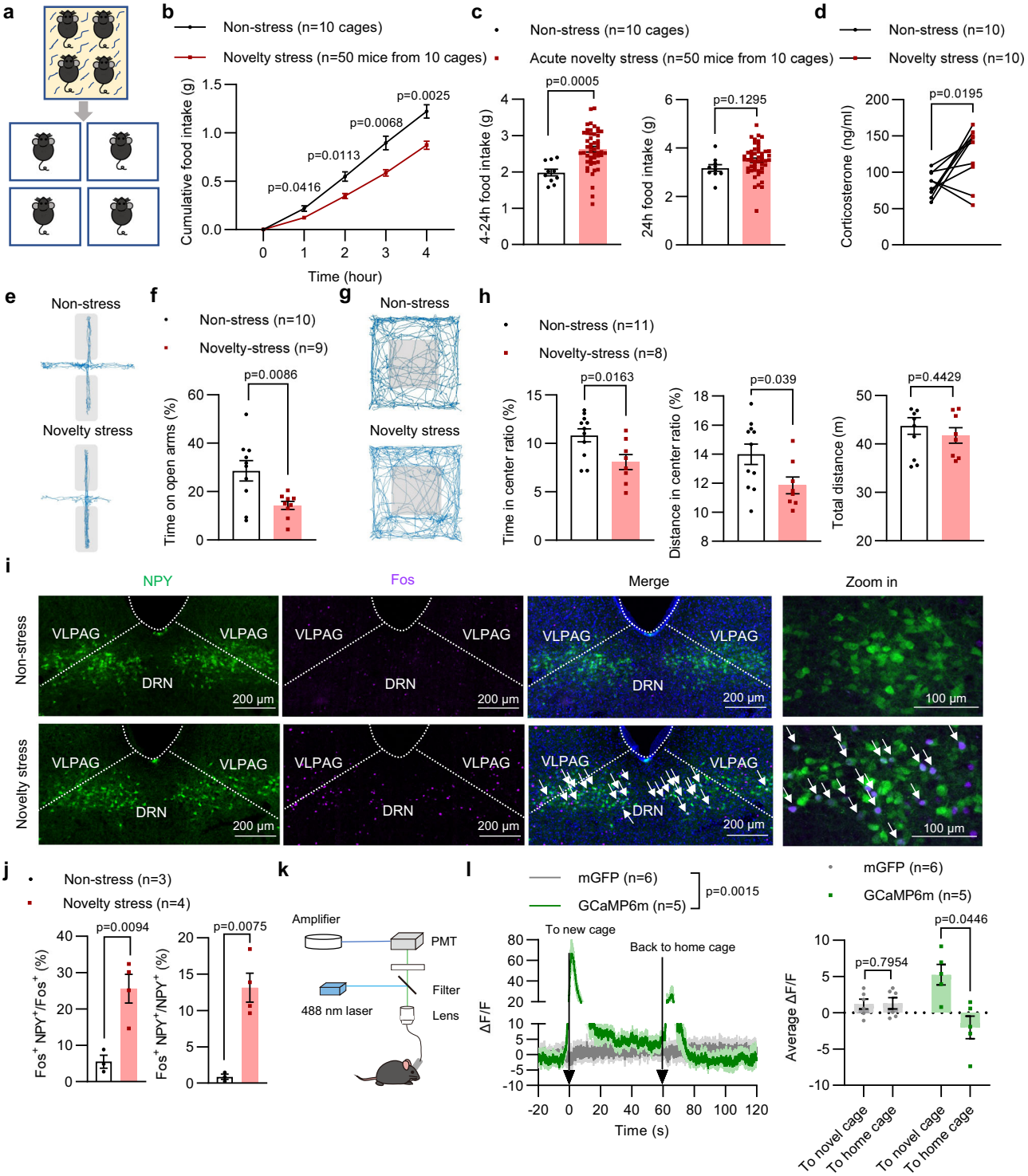

Fig. 1 | Acute novelty stress decreases food intake, induces anxiety and activates NPY$^{DRN/vlPAG}$ neurons. a Acute novelty stress paradigm. Group-housed mice were individually transferred into new cages without padding to induce acute novelty stress. 4-h (**b**), 4–24-h (**c**) and 24-h (**c**) food intake under acute novelty stress and non-stress conditions. n = 10 cages (50 mice) for non-stress group and n = 50 mice for novelty stress group. In this study, the food intake of group-housed mice was calculated by dividing the total food per cage by mice number in the cage. In (**b**) Two-way ANOVA with post-hoc Šídák's multiple comparisons test. In (**c**) Two-sided unpaired Student's *t* test. **d** The levels of serum corticosterone before and after 1 h after novelty stress. Two-sided paired Student's *t* test. **e** Representative elevated plus maze (EPM) traces of non-stress and novelty stress groups. The gray shades indicate the closed arms. **f** Percentages of open-arm time in the EPM. Two-sided unpaired Student's *t* test with Welch's correction. **g** Representative open field test (OFT) traces of non-stress and novelty stress groups. The gray shades indicate the center arena. **h** Percentages of time, travel distance in the center area and total travel distance of OFT. Two-sided unpaired Student's *t* test. **i** 2-h novelty stress induced Fos (purple) signals in NPY$^{DRN/vlPAG}$ neurons (green) from *Npy*^{GFP} mice. Representative images (**i**) and quantitative data (**j**). In (**i**), blue represents DAPI staining and arrows indicate Fos$^+$NPY$^+$ neurons. The rightmost panels are magnified images. In (**j**), for percentage among Fos$^+$ neurons, two-sided unpaired Student's *t* test; For percentage among NPY$^+$ neurons, two-sided unpaired Student's *t* test with Welch's correction. **k** Fiber photometry recording setup. **l** NPY$^{DRN/vlPAG}$ calcium signals in mice individually transferred to a novel cage without padding for 1 min and back to home cages. Two-way ANOVA with post-hoc Šídák's multiple comparisons test. Right: Average calcium changes when mice were in new cages (20–40 s) and home cages (80–100 s). Two-sided paired Student's *t* test. Data are shown as mean ± SEM. Unless specified, 'n' refers to mice number. Source data are provided as a Source Data file.

stress to inhibit NPY$^{DRN/vlPAG}$ neurons in advance (Supplementary Fig. 3c). Interestingly, inhibiting NPY$^{DRN/vlPAG}$ neurons not only significantly exacerbated novelty stress-induced hypophagia in the first 4 hs (Fig. 2c) but also decrease 24-h total food intake over the whole stress period (Fig. 2d). These results suggested that the inhibition of NPY$^{DRN/vlPAG}$ neurons worsens acute novelty stress-induced hypophagia.

To activate NPY$^{DRN/vlPAG}$ neurons, a Cre-dependent excitatory chemogenetic vector, AAV-DIO-hM3Dq-mCherry, was injected into the DRN/vlPAG region of *Npy*$^{ires\text{-}Cre}$ mice (referred to as NPY^{hM3Dq} mice). In vitro electrophysiological recordings confirmed that CNO successfully activated NPY^{hM3Dq} neurons with increased neuronal membrane potential and firing frequency (Fig. 2e and Supplementary Fig. 3b). FISH results showed that the majority (~85%, 313 neurons from 3 brain slices) of hM3Dq^{+} neurons co-expressed *Npy* (Fig. 2f). Strikingly, activation of NPY$^{DRN/vlPAG}$ neurons by CNO injection (i.p., 2 mg/kg) half an hour before novelty stress completely reversed novelty stress-induced hypophagia in the first 4 hs (Supplementary Fig. 3c and Fig. 2g). There were no changes in 24-h food intake with NPY$^{DRN/vlPAG}$ neural activation by novelty stress (Fig. 2h). We injected AAV-DIO-mCherry into the DRN/vlPAG region of *Npy*$^{ires\text{-}Cre}$ mice (NPY^{mCherry} mice) as an additional control. CNO injections did not affect stress-induced hypophagia in NPY^{mCherry} mice, suggesting that the observed phenotypes were not due to any off-target effects of CNO or its derivates (Fig. 2i, j). These results suggest that NPY$^{DRN/vlPAG}$ neurons are sufficient to resist novelty stress-induced acute hypophagia without altering the total food intake in 24 hs, thereby serving as stress response-resisting neuronal groups.

NPY$^{DRN/vlPAG}$ neurons do not affect homeostatic food intake

NPY is a potent appetite-stimulating hormone and NPY neurons in many brain areas are known to drive homeostatic feeding[27,28]. We next evaluated whether NPY$^{DRN/vlPAG}$ neurons affect homeostatic feeding behaviors. Firstly, NPY$^{DRN/vlPAG}$ neurons were not activated by fasting or fasting-refeeding (Supplementary Fig. 3d, e). Secondly, chemogenetic inhibition of NPY$^{DRN/vlPAG}$ neurons had no impact on refeeding intake after an overnight fast (Supplementary Fig. 3f), suggesting that these NPY$^{DRN/vlPAG}$ neurons are not required for mounting refeeding after a fast.

To examine whether NPY$^{DRN/vlPAG}$ neurons regulate ad libitum feeding or body weight homeostasis, we injected CNO (i.p., 2 mg/kg) into NPY^{hM3Dq} mice once daily for 14 consecutive days without any artificial stress. AAV-DIO-mGFP was injected into the DRN/vlPAG of *Npy*$^{ires\text{-}cre}$ mice (NPY^{mGFP} mice) as a control. There was no significant difference in food intake and body weight changes between NPY^{hM3Dq} mice and control mice during the whole 14 days (Supplementary Fig. 3g, h). Interestingly, on day 1, probably due to an indirect injection stress, we observed a slight decrease in food intake of NPY^{mGFP} mice compared with the NPY^{hM3Dq} mice (Supplementary Fig. 3g). However, from day 2 onward, as mice acclimated to the injection stress, there was no significant difference between the groups. Moreover, the food intake of NPY^{hM3Dq} mice on day 1 did not differ from that on subsequent days, indicating that activating NPY$^{DRN/vlPAG}$ neurons does not increase absolute food intake. These results indicated that the effect of NPY$^{DRN/vlPAG}$ neuron activation on increased food intake is specific to feeding during stress and NPY$^{DRN/vlPAG}$ neurons have no effects on homeostatic feeding behaviors.

To further determine whether NPY$^{DRN/vlPAG}$ neurons are required for ad libitum feeding or body weight homeostasis, we selectively ablated these neurons using a caspase 3-mediated strategy[29]. We bred *Npy*$^{ires\text{-}Cre}$ mice with Ai14 reporter mice to track and visualize NPY neurons (referred to as *Npy*$^{ires\text{-}Cre}$*::Rosa26*^{Ai14} mice). In *Npy*$^{ires\text{-}Cre}$*::Rosa26*^{Ai14} mice, about 70% Ai14^{+} neurons co-expressed *Npy* (Supplementary Fig. 3i). The AAV-DIO-taCaspase3 viral vectors were bilaterally injected into the DRN/vlPAG region of *Npy*$^{ires\text{-}Cre}$*::Rosa26*^{Ai14} mice to ablate NPY$^{DRN/vlPAG}$ neurons (Supplementary Fig. 3j). Cre^{-} littermates with Caspase3 injection were used as control mice. Caspase 3-mediated ablation of NPY$^{DRN/vlPAG}$ neurons showed no effect on daily ad libitum food intake and body weight over 7 weeks (Supplementary Fig. 3k, l). These results demonstrated that NPY$^{DRN/vlPAG}$ neurons are not required for maintaining ad libitum feeding and body weight homeostasis.

Activation of NPY$^{DRN/vlPAG}$ neurons attenuates anxiety during acute novelty stress

Next, we investigated whether NPY$^{DRN/vlPAG}$ neurons affect other stress responses. We found that chemogenetic activation of NPY$^{DRN/vlPAG}$ neurons significantly reduced the number of 2-h novelty stress-induced Fos^{+} neurons in the PVN (Fig. 3a, b), a key brain area in mediating stress response. Accordingly, NPY$^{DRN/vlPAG}$ neuron activation tended to suppress the novelty stress-induced increase in corticosterone levels (Fig. 3c), although it did not reach statistical significance. Directly activating NPY$^{DRN/vlPAG}$ neuron in conditions of a homeostatic state had no effects on corticosterone levels (Supplementary Fig. 3m), indicating a stress-specific role of NPY$^{DRN/vlPAG}$ neurons. These data suggested that NPY$^{DRN/vlPAG}$ neurons might prevent the overactivation of the hypothalamus-pituitary-adrenal (HPA) axis during stress.

We then asked whether activation of NPY$^{DRN/vlPAG}$ neurons can ameliorate novelty stress-induced anxiety-like behaviors using the EPM and the OFT. Mice were injected with CNO (i.p., 2 mg/kg) half an hour before a 2-h acute novelty stress exposure, followed by assessment of anxiety-like behaviors (Fig. 3d). While chemogenetically enhancing the activation of NPY$^{DRN/vlPAG}$ neurons only mildly increased the time mice spent on the open arm of the EPM (Fig. 3e, f), it did significantly increase OFT center time in novelty stress-exposed mice (Fig. 3g, h). In contrast, chemogenetic inhibition of NPY$^{DRN/vlPAG}$ neurons had no significant impact on anxiety in novelty stress-exposed mice, as assessed by the EPM and the OFT (Fig. 3e-h). These data suggested that activation of NPY$^{DRN/vlPAG}$ neurons may at least partially ameliorate acute novelty stress-induced anxiety-like behaviors.

NPY$^{DRN/vlPAG}$ neurons are essential for resisting chronic restraint stress-induced hypophagia and anxiety

To examine whether NPY$^{DRN/vlPAG}$ neurons play a role in resisting or adapting to chronic stress, which often leads to more disease-related effects[30], we introduced chronic restraint stress, another common stress paradigm that causes hypophagia and body weight loss[31]. In addition, chronic restraint stress induces anxiety[32] and/or depression[33] phenotypes, which mimics psychiatric diseases induced by stressful environments in human society. For this chronic stress, we challenged mice with 2–3 hs daily restraint sessions for 14 days (Fig. 4a). Consistent with previous studies[34], a 14-day consecutive restraint stress caused a significant reduction in food intake and body weight (Fig. 4b, c). Meanwhile, there was a remarkable increase of the corticosterone level after the first day of restraint, which maintained elevated even after 14 days of stress (Fig. 4d). Interestingly, the mice showed a recovery in feeding from day 10, which is supported by other studies[31,35] and may be partly due to habituation to the repeated stress[36]. Though food intake slightly increased from day 11 to day 14 of restraint stress, it did not reach the level of the non-stressed control group. Accordingly, their body weight kept decreasing during the whole restraint test period, albeit with a slower decreasing rate in the second week. After the end of restraint stress, 24-h food intake of non-restraint and 14-day restraint-treated mice remained comparable (Supplementary Fig. 4a).

We then employed Fos immunostaining and in vivo fiber photometry calcium imaging to examine the neuronal activity of NPY$^{DRN/vlPAG}$ neurons during restraint stress. Fos immunostaining demonstrated

https://doi.org/10.1038/s41467-024-51956-9

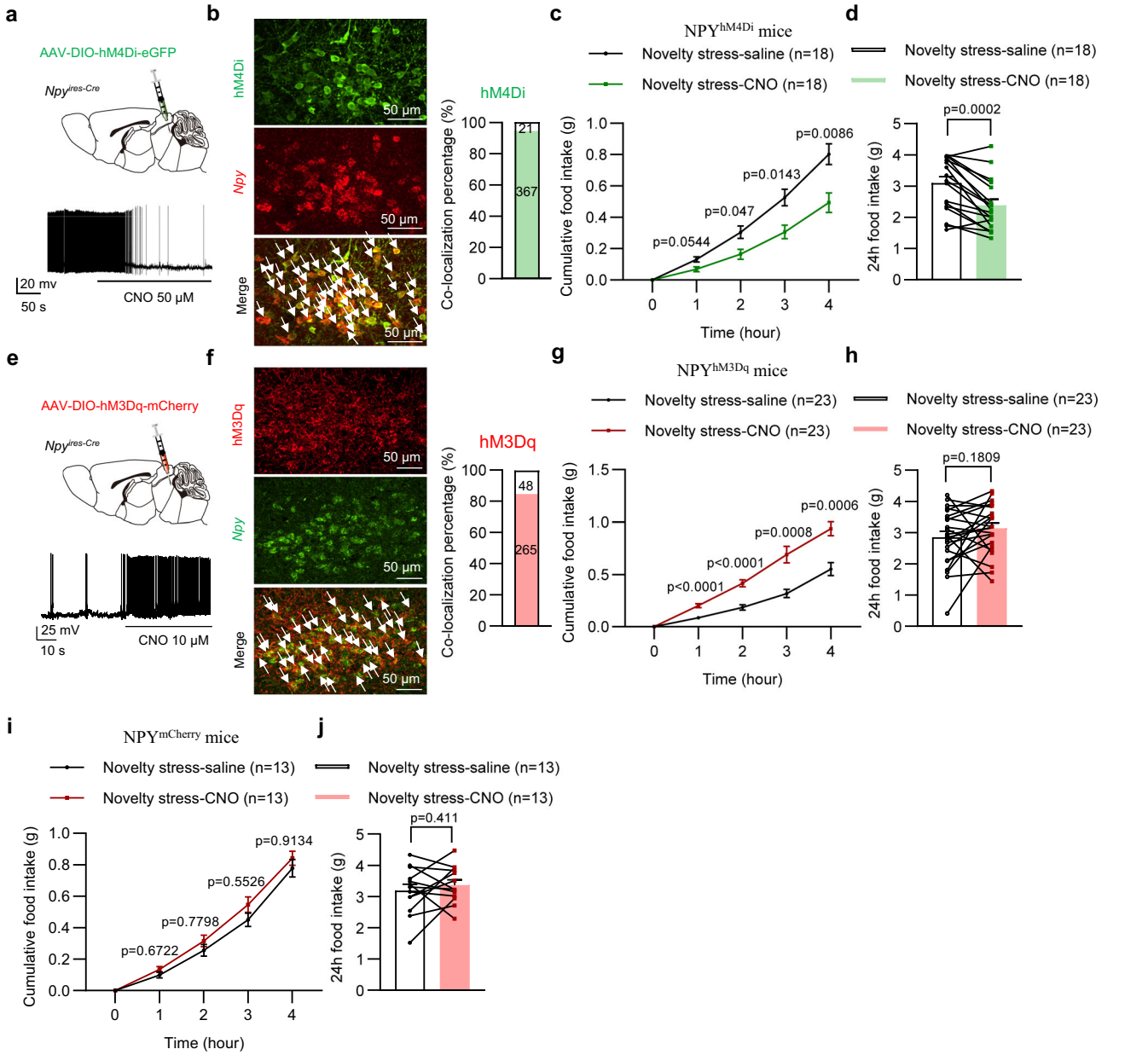

Fig. 2 | NPY$^{DRN/vlPAG}$ neurons regulate the hypophagic response to acute novelty stress. a Viral injection and representative current clamp recording of a NPY^{hM4Di} neuron with the bath of 50 μM clozapine N-oxide (CNO). **b** Fluorescence in situ hybridization (FISH) images showing colocalization of hM4Di (green) and *Npy* (red) mRNA. Arrows indicate hM4Di^{+}*Npy*$^{+}$ neurons. In 388 hM4Di^{+} neurons, 367 of them co-express *Npy*. The experiment was repeated 2 times with similar results. 4-h (**c**) and 24-h (**d**) food intake of NPY^{hM4Di} mice under acute novelty stress. In (**c**) Two-way ANOVA with post-hoc Šídák's multiple comparisons test. In (**d**) Two-sided Wilcoxon matched-pairs signed rank test. **e** Viral injection and representative current clamp recording of a NPY^{hM3Dq} neuron with the bath of 10 μM CNO. **f** FISH images showing colocalization of hM3Dq (red) and *Npy* (green) mRNA. Arrows indicate hM3Dq^{+}*Npy*$^{+}$ neurons. In 313 hM3Dq^{+} neurons, 265 of them co-express *Npy*. The experiment was repeated 2 times with similar results. 4-h (**g**) and 24-h (**h**) food intake of NPY^{hM3Dq} mice under acute novelty stress. In (**g**) Two-way ANOVA with post-hoc Šídák's multiple comparisons test. In (**h**) Two-sided paired Student's *t* test. 4-h (**i**) and 24-h (**j**) food intake of NPY^{mCherry} mice under acute novelty stress. In (**i**) Two-way ANOVA with post-hoc Šídák's multiple comparisons test. In (**j**) Two-sided paired Student's t test. Data are shown as mean ± SEM. 'n' refers to mice number. Source data are provided as a Source Data file.

that these NPY$^{DRN/vlPAG}$ neurons were strongly activated by 2-h restraint stress (Fig. 4e, f). Consistent with Fos immunostaining result, acute restraint rapidly activated NPY$^{DRN/vlPAG}$ neurons in the in vivo fiber photometry imaging (Fig. 4g). To examine the role of NPY$^{DRN/vlPAG}$ neurons in chronic restraint stress, we chronically inhibited NPY$^{DRN/vlPAG}$ neurons by daily injection of NPY^{hM4Di} mice or NPY^{mCherry} control mice with clozapine (i.p., 0.2 mg/kg) half an hour prior to everyday restraint (Fig. 4h). Clozapine has been shown to produce less side effects than CNO for long-term chemogenetic manipulation[37]. We confirmed that 5 μM clozapine effectively inhibited hM4Di^{+} NPY$^{DRN/vlPAG}$ neurons with decreased neuronal membrane potential and firing frequency (Supplementary Fig. 4b, c). As a result, NPY^{hM4Di} mice consumed less food and lost more body weight than NPY^{mCherry} mice during chronic restraint stress (Fig. 4i, j), indicating that chemogenetic inhibition of NPY$^{DRN/vlPAG}$ neurons exacerbated chronic restraint stress-induced hypophagia. In addition, NPY^{hM4Di} mice had a significantly decreased center time/distance in the OFT compared with NPY^{mCherry} mice (Fig. 4k). There was no significant difference in EPM open-arm time (Fig. 4l). Notably, despite the exacerbation of anxious states, inhibiting NPY$^{DRN/vlPAG}$ neurons during 14-day restraint stress did not further

https://doi.org/10.1038/s41467-024-51956-9

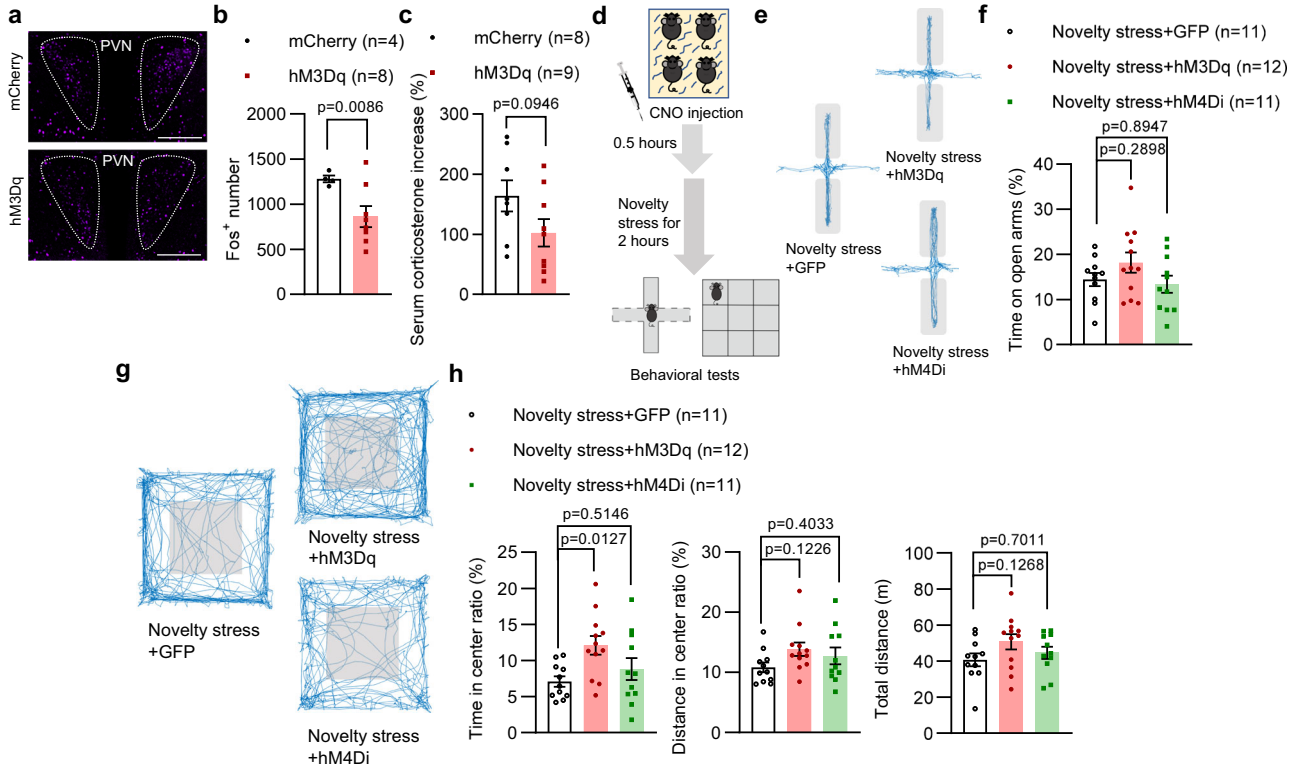

Fig. 3 | Activation of NPY$^{DRN/vlPAG}$ neurons ameliorates stress-induced anxiety-like behaviors. a Acute novelty stress-induced Fos (purple) signals in the paraventricular hypothalamic nucleus (PVN) of CNO-treated NPY^{mcherry} and NPY^{hM3Dq} mice. Representative images (**a**) and quantitative data (**b**). Scale bar: 200 μm. In (**b**) Two-sided unpaired Student's *t* test with Welch's correction. **c** The increase of serum corticosterone levels caused by novelty stress in CNO-treated NPY^{mCherry} and NPY^{hM3Dq} mice. Two-sided unpaired Student's *t* test. **d** Schematic of behavioral test design after 2-h acute novelty stress with chemogenetic manipulation. **e** Representative EPM traces of different mouse groups. The gray shades indicate the closed arms. **f** Percentages of open-arm time in the EPM. Ordinary one-way ANOVA with post-hoc Dunnett's multiple comparisons test. **g** Representative OFT traces of different mouse groups. The gray shades indicate the center of the arena. **h** Percentages of time, travel distance in the center area and total travel distance in OFT. Ordinary one-way ANOVA with post-hoc Dunnett's multiple comparisons test. Stressed mice were subjected to acute novelty stress for 2 hs prior to behavioral tests, and all stressed mice received CNO injections. Data are shown as mean ± SEM. 'n' refers to mice number. Source data are provided as a Source Data file.

increase corticosterone levels (Supplementary Fig. 4d). Together these data suggested that NPY$^{DRN/vlPAG}$ neurons are essential for resisting chronic restraint stress-induced hypophagia and anxiety.

NPY in NPY$^{DRN/vlPAG}$ neurons is critical for the anxiolytic effects

To further determine the responsibility of NPY in the NPY$^{DRN/vlPAG}$ neurons for the anxiolytic effects observed above, we injected AAV-Cre-GFP into the DRN/vlPAG of *Npy*$^{lox/lox}$ mice[4] to selectively knockdown NPY expression in the DRN/vlPAG (Fig. 5a). Mice receiving a Cre injection showed a significant reduction of NPY expression as compared to mCherry controls (Fig. 5a, b and Supplementary Fig. 4e). Knocking down NPY$^{DRN/vlPAG}$ did not affect normal body weight gain (Fig. 5c) and daily food intake (Fig. 5d), indicating that NPY in the DRN/vlPAG is not involved in the homeostatic regulation of body weight and food intake. However, during acute novelty stress, knocking down NPY significantly decreased 4-h food intake (Fig. 5e) with no recovery in the following 4-24 hs (Supplementary Fig. 4f). Moreover, NPY$^{DRN/vlPAG}$-knockdown mice showed trends towards increased anxiety as reflected by decreased center time and traveled distance in the OFT compared to control mice after acute novelty stress (Fig. 5f). There was no difference in the EPM test between NPY knockdown and control mice (Fig. 5g). These results suggested that NPY in the DRN/vlPAG is critical for resisting acute novelty stress-induced hypophagia and anxiety.

On the other hand, within the chronic restraint stress paradigm, there was still no significant change in body weight between NPY$^{DRN/vlPAG}$-knockdown mice and control mice (Fig. 5h). Consistent with acute stress, NPY$^{DRN/vlPAG}$-knockdown mice exhibited a significantly decreased center time/traveled distance compared with control mice in the OFT (Fig. 5i). We did not observe any significant difference in the EPM, either (Fig. 5j). These results suggested that NPY in the DRN/vlPAG plays a crucial role for mitigating stress-induced anxiety under chronic stress conditions.

Optogenetic activation of NPY$^{DRN/vlPAG}$ neurons attenuates stress-induced hypophagia and transmit positive valence

To evaluate instantaneous anti-stress effects of NPY$^{DRN/vlPAG}$ neurons, we employed optogenetic activations of NPY$^{DRN/vlPAG}$ neurons. AAV-DIO-hChR2-mCherry was injected into the DRN/vlPAG region of *Npy*$^{ires\text{-}Cre}$ mice (referred to as NPY^{hChR2} mice, Fig. 6a). The majority of hChR2^{+} neurons (~80%, 178 neurons from 3 brain slices) co-expressed *Npy* (Fig. 6b), confirming the expressional accuracy of hChR2 virus. During the whole optogenetic experiments, NPY^{hChR2} mice were singly placed in testing chambers, which mimiced an acute novelty stress environment and thus mice ate little food (Supplementary Fig. 5a). As expected, optogenetic activation of NPY$^{DRN/vlPAG}$ neurons (10 mW power, 10 ms pulse, 1-s on and 1-s off) with either 5, 10, or 20 Hz frequency increased 1-h food intake compared with no-light condition (Supplementary Fig. 5b). In contrast to chemogenetic manipulation, light activation throughout the 2-h novelty stress did not alter time spent in the open arm of the EPM or in the center of the OFT (Supplementary Fig. 5c, d). Only total distance in the OFT significantly increased (Supplementary Fig. 5c), which may be the result of light-evoked brain heating and phototoxicity[38].

https://doi.org/10.1038/s41467-024-51956-9

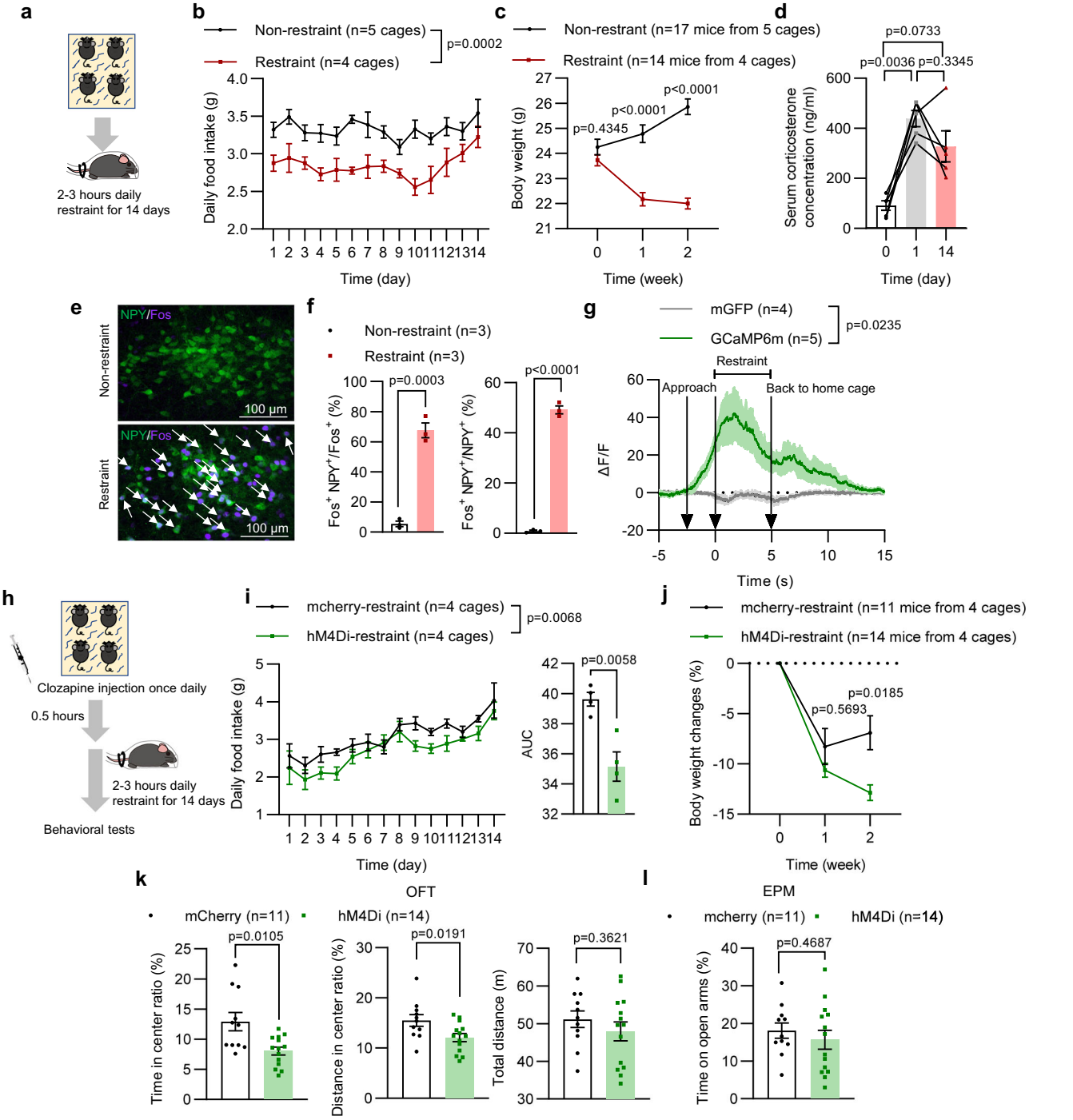

Fig. 4 | NPY$^{DRN/vlPAG}$ neurons are essential for chronic restraint stress-induced hypophagia and anxiety. a Experimental strategy for 14-day restraint stress. Daily food intake (**b**) and body weight (**c**) of non-restraint and 14-day restraint-treated mice. n = 17 mice from 5 cages for non-restraint group, n = 14 mice from 4 cages for restraint group. Two-way ANOVA with post-hoc Šídák's multiple comparisons. **d** The levels of serum corticosterone in mice at day 0, day 1, and day 14 of the 14-day restraint stress. n = 5 mice. Repeated measures one-way ANOVA with post-hoc Tukey's multiple comparisons test. **e** 2-h restraint stress induced Fos (purple) signals in NPY$^{DRN/vlPAG}$ neurons (green) from *Npy*^{GFP} mice. Representative images (**e**) and quantitative data (**f**). In (**e**), Arrows indicate NPY^{+}Fos^{+} neurons. In (**f**) Two-sided unpaired Student's *t* test. **g** NPY$^{DRN/vlPAG}$ neuronal calcium signals in response to restraint stress. Two-way ANOVA with post-hoc Šídák's multiple comparisons test. **h** Experimental strategy for 14-day restraint stress with chemogenetic inhibition. **i** Daily food intake and its area under curve (AUC) of mCherry-restraint and hM4Di-restraint mice during 14 days of restraint stress. For the daily food intake, two-way ANOVA with post-hoc Šídák's multiple comparisons test. For the daily food intake AUC, two-sided unpaired Student's *t* test. **j** Percentage of body weight changes of mCherry-restraint and hM4Di-restraint mice during 14 days of restraint stress. Two-way ANOVA with post-hoc Šídák's multiple comparisons test. **k**, **l** Behavioral tests of mCherry and hM4Di mice after 14 days of restraint stress. **k** Percentages of time, travel distance in the center area and total travel distance in OFT. **l** Percentages of open-arm time in EPM. For percentage of time in the center area of OFT, two-sided unpaired Student's *t* test with Welch's correction; For the others, two-sided unpaired Student's *t* test. All restraint mice in (**i**–**l**) received clozapine once daily for 14 days. Data are shown as mean ± SEM. Unless specified, 'n' refers to mice number. Source data are provided as a Source Data file.

https://doi.org/10.1038/s41467-024-51956-9

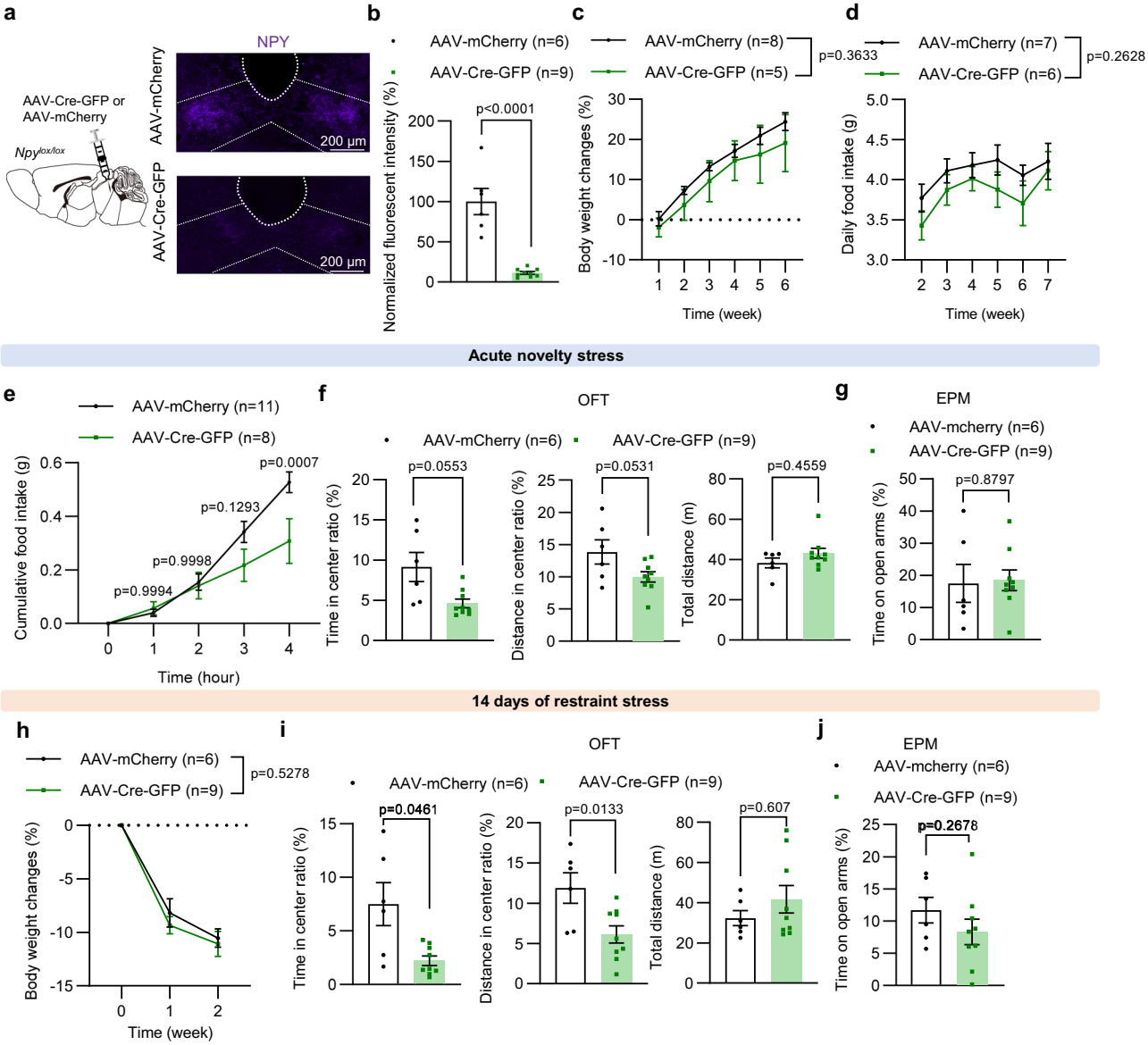

Fig. 5 | NPY knockdown in DRN/vlPAG exacerbates stress-induced anxiety. **a** Representative images of NPY$^{DRN/vlPAG}$ expression (purple) from a AAV-mCherry or AAV-Cre-GFP virus-injected *Npy*$^{lox/lox}$ mouse. **b** Quantification of NPY fluorescent intensity percentage between AAV-mCherry and AAV-Cre-GFP *Npy*$^{lox/lox}$ groups. Two-sided unpaired Student's *t* test. **c** Percentage of body weight changes of group-housed AAV-mCherry and AAV-Cre-GFP *Npy*$^{lox/lox}$ groups. Two-way ANOVA with post-hoc Šídák's multiple comparisons test. **d** Average daily food intake of individual-housed AAV-mCherry and AAV-Cre-GFP *Npy*$^{lox/lox}$ groups. Two-way ANOVA with post-hoc Šídák's multiple comparisons test. **e** 4-h food intake of AAV-mCherry and AAV-Cre-GFP *Npy*$^{lox/lox}$ groups under acute novelty stress. Two-way ANOVA with post-hoc Šídák's multiple comparisons test. **f**, **g** Behavioral tests of AAV-mCherry and AAV-Cre-GFP *Npy*$^{lox/lox}$ groups after novelty stress. **f** Percentages of time, travel distance in the center area and total travel distance in OFT after acute novelty stress. **g** Percentages of open-arm time in EPM. For percentage of time in the center area of OFT, two-sided unpaired Student's *t* test with Welch's correction; For total distance of OFT, two-sided Mann Whitney test; For the others, two-sided unpaired Student's *t* test. **h** Percentage of body weight changes of AAV-mCherry and AAV-Cre-GFP *Npy*$^{lox/lox}$ groups during 14 days of restraint stress. Two-way ANOVA with post-hoc Šídák's multiple comparisons test. **i**, **j** Behavioral tests of AAV-mCherry and AAV-Cre-GFP *Npy*$^{lox/lox}$ groups after 14 days of restraint stress. **i** Percentages of time, travel distance in the center area and total travel distance in OFT. **j** Percentages of open-arm time in EPM. For percentage of time in the center area of OFT, two-sided unpaired Student's *t* test with Welch's correction; For total distance of OFT, two-sided Mann Whitney test; For the others, two-sided unpaired Student's *t* test. Data are shown as mean ± SEM. 'n' refers to mice number. Source data are provided as a Source Data file.

Positive emotional valence is important for stress resistance. Next, we explored the emotional valence of NPY$^{DRN/vlPAG}$ neurons by testing mice in a two-chamber real-time place preference test (RTPP). Apart from optogenetic activation, we injected AAV-DIO-GtACR1-eGFP into the DRN/vlPAG region of *Npy*$^{ires\text{-}Cre}$ mice (referred to as NPY^{GtACR1} mice) to optogenetically inhibit NPY$^{DRN/vlPAG}$ neurons (Fig. 6a). FISH results confirmed that the majority of GTACR1^{+} neurons (~95%, 195 neurons from 4 brain slices) co-expressed *Npy* (Fig. 6b). The RTPP test consisted of three 15-min sessions: Pre-stimulation, stimulation and post-stimulation periods. In the stimulation session, once the mice moved to the laser-paired side, the laser was turned on (10 mW, 20 Hz, 10 ms pulse, 1-s on and 1-s off for NPY^{hChR2} mice and 3 mW for NPY^{GtACR1} mice). Interestingly, NPY^{hChR2} mice exhibited a significant preference for the laser stimulation-paired chamber (Fig. 6c, d), whereas NPY^{GtACR1} mice exhibited a significant aversion to the laser stimulation-paired chamber (Fig. 6c, e). Laser stimulation did not produce preference or aversion in mCherry injected control mice (Fig. 6f). These results suggested that

https://doi.org/10.1038/s41467-024-51956-9

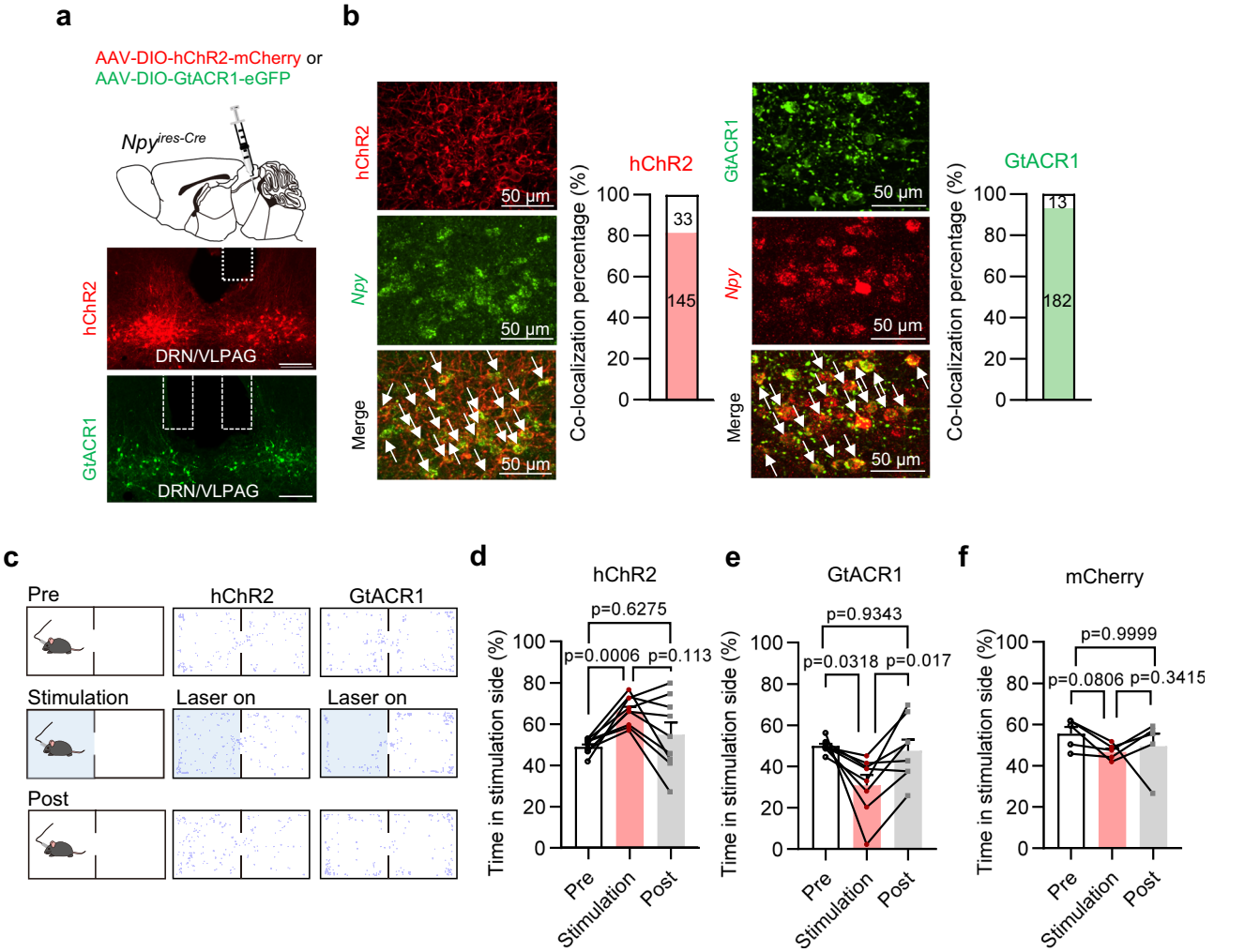

Fig. 6 | NPY$^{DRN/vlPAG}$ neurons transmit positive valence. a Optogenetic manipulation of NPY^{hChR2} and NPY^{GtACR1} neurons. Representative images showing hChR2 expression (red), GtACR1 expression (green) and optical fiber placements (white dashed line). Scale bar: 200 μm. **b** Representative FISH images showing colocalization of hChR2/GtACR1 and *Npy* mRNA. In 178 hChR2$^+$ neurons, 145 of them co-express *Npy*. In 195 GtACR1$^+$ neurons, 182 of them co-express *Npy*. Arrows indicate hChR2$^+$*Npy*$^+$ or GtACR1$^+$*Npy*$^+$ neurons. The experiment was repeated 2 times with similar results. **c** Representative locomotor traces of NPY^{hChR2} and NPY^{GtACR1} mice before, during and after laser stimulation. Percentages of time in the stimulation side of NPY^{hChR2} mice (**d**), NPY^{GtACR1} mice (**e**), and NPY^{mCherry} mice (**f**) during real-time place preference test (RTPP). In (**d**), n = 9 mice, repeated measures one-way ANOVA with post-hoc Tukey's multiple comparisons test. In (**e**), n = 8 mice, repeated measures one-way ANOVA with post-hoc Tukey's multiple comparisons test. In (**f**), n = 5 mice, two-sided Friedman test with post-hoc Dunn's multiple comparisons test. Data are shown as mean ± SEM. 'n' refers to mice number. Source data are provided as a Source Data file.

NPY$^{DRN/vlPAG}$ neurons transmit positive emotional valence, which further supports their anxiolytic effects.

The NPY$^{DRN/vlPAG}$ → PVT and NPY$^{DRN/vlPAG}$ → LH neural circuits

To elucidate the neural circuits engaged by NPY$^{DRN/vlPAG}$ neurons in mediating anxiolytic effects, we used a Cre-dependent, synapse-specific anterograde AAV viral tracer (AAV-DIO-mGFP-2A-Synaptophysin-mRuby) to investigate the projection patterns of these neurons[39] (Fig. 7a). This strategy allowed the specific examination of mRuby expression in presynaptic terminals, thereby indicating potential functional synaptic connections. In total, NPY$^{DRN/vlPAG}$ neurons projected to approximately 18 downstream areas (Table 1), including several stress-related brain regions such as the MPA/lateral preoptic area (LPO), the PVT, the LH[40], the anterior hypothalamic area/lateroanterior hypothalamic nucleus (AH/LA)[41] and the dorsomedial hypothalamic nucleus (DMH)[42] (Fig. 7b). However, we observed almost no or only minimal NPY$^{DRN/vlPAG}$-derived projections to the PVN, the arcuate nucleus (ARC), the central amygdaloid nucleus (CeA), the BLA, and the nucleus accumbens (Acb) (Supplementary Fig. 6a).

We then used optogenetics-assisted circuit mapping to study the functional effects of these NPY$^{DRN/vlPAG}$-derived projections. Optical fibers were placed in the MPA/MPO, the PVT, the LH, the AH/LA, or the DMH for terminal stimulations (Supplementary Fig. 6b). We found that although no difference was observed in other areas, optogenetic activation (10 mW, 20 Hz, 10 ms pulse, 1-s on and 1-s off, 1 h) of the NPY$^{DRN/vlPAG}$-derived projections in the PVT significantly stimulated feeding (Fig. 7c), suggesting a role for the NPY$^{DRN/vlPAG}$ → PVT circuit to resist stress-induced suppression of feeding. On the other hand, different from other projections, only activation (10 mW, 20 Hz, 10 ms pulse, 1-s on and 1-s off) of NPY$^{DRN/vlPAG}$ derived projections in the LH produced a significant preference for the laser stimulation-paired chamber (Fig. 7d), suggesting that NPY$^{DRN/vlPAG}$ neurons could convey positive valence against stress via the projections to the LH.

Since PVT and LH separately functioned in stress resistance, we sought to explore whether PVT-projecting and LH-projecting NPY$^{DRN/vlPAG}$ neurons represented two distinct subgroups. AAV-retro-DIO-EGFP and AAV-retro-DIO-m_Tdtomato were injected into PVT and LH of *Npy*$^{ires-Cre}$

https://doi.org/10.1038/s41467-024-51956-9

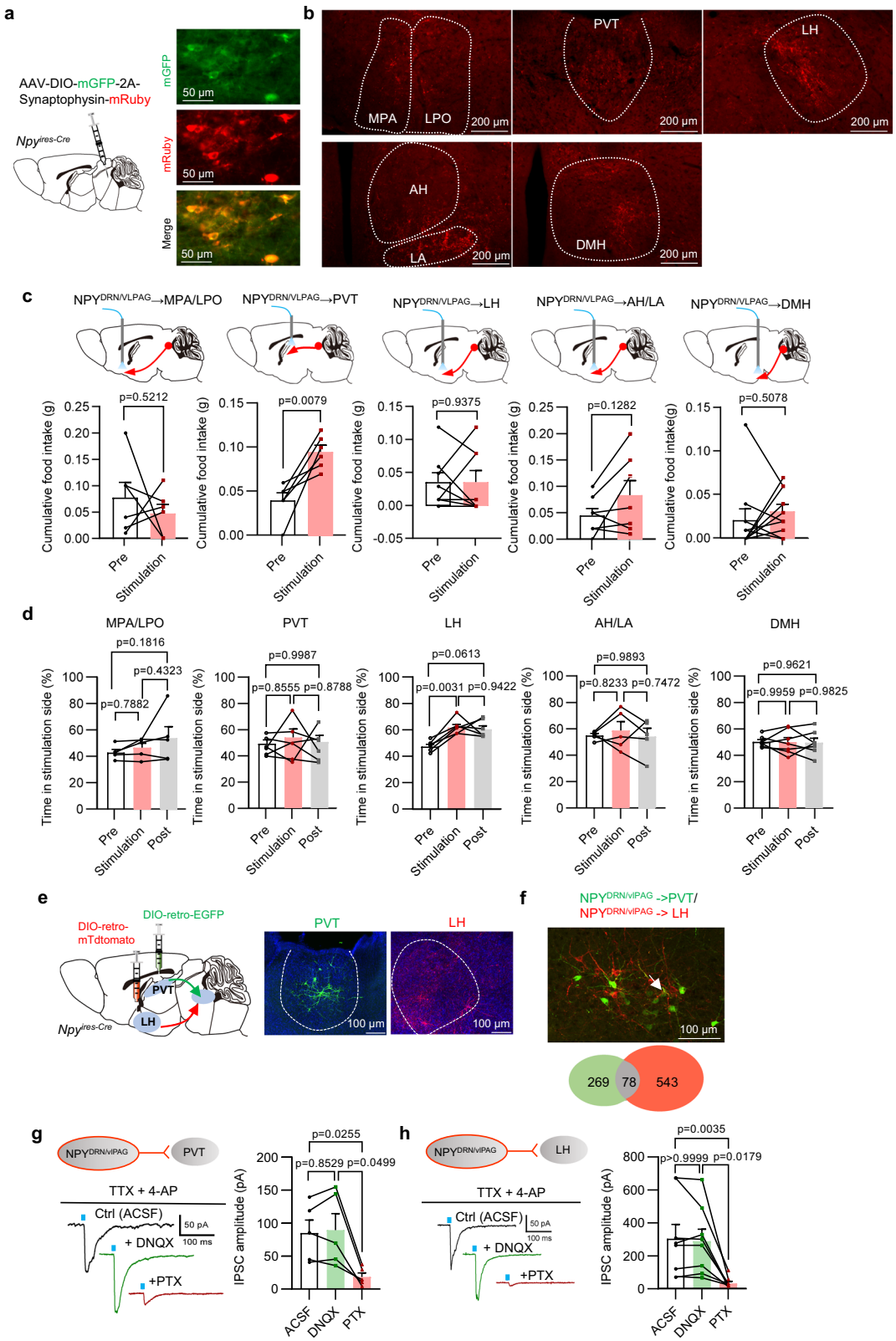

Fig. 7 | NPY$^{DRN/vlPAG}$ neurons regulate feeding behaviors and positive valence via different neural pathways. AAV virus-based anterograde tracing. **a** Representative images showing mGFP and mRuby expression in NPY$^{DRN/vlPAG}$ neurons. **b** Representative images showing NPY$^{DRN/vlPAG}$ neuron-derived projections (red) in multiple brain regions. The experiment was repeated 4 times with similar results. **c** 1-h food intake in mice fed ad libitum before and during optogenetic activation of NPY$^{DRN/vlPAG}$ neuronal terminals in downstream brain regions. For the lateral hypothalamic area (LH) and the dorsomedial hypothalamic nucleus (DMH) stimulation data, two-sided Wilcoxon matched-pairs signed rank test; For the others, two-sided paired Student's *t* test. The medial/lateral preoptic area (MPA/LPO): n = 6 mice; The paraventricular thalamic nucleus (PVT): n = 6 mice; LH: n = 8 mice; The anterior hypothalamic area/lateroanterior hypothalamic nucleus (AH/LA): n = 7 mice; DMH: n = 10 mice. **d** Percentages of time in the stimulation side of RTPP with NPY$^{DRN/vlPAG}$-terminals optogenetic activation. Repeated measures one-way ANOVA with post-hoc Tukey's multiple comparisons test. MPA/LPO: n = 5 mice; PVT: n = 6 mice; LH: n = 6 mice; AH/LA: n = 5 mice; DMH: n = 7 mice. **e** Virus injection strategy to retrogradely label PVT- and LH- projecting NPY$^{DRN/vlPAG}$ neurons and representative images showing PVT- (green) and LH- (red) projecting NPY neuronal terminals. **f** Representative images showing NPY$^{DRN/vlPAG}$ neurons retrogradely labeled from PVT (green) and LH (red). Arrow indicates double-labeled neuron. Bottom: Total numbers of PVT- (green), LH- (red) projecting and PVT/LH- dual projecting NPY$^{DRN/vlPAG}$ neurons (n = 4 mice). Representative traces and quantification of light-evoked postsynaptic current amplitude of NPY$^{DRN/vlPAG}$-PVT (**g**) or NPY$^{DRN/vlPAG}$-LH (**h**) connectivity with application of DNQX or picretoxin (PTX). The blue lines indicate 5-ms light pulse. In (**g**), n = 5 cells, repeated measures one-way ANOVA with post-hoc Tukey's multiple comparisons test; In (**h**), n = 8 cells, two-sided Friedman test with post-hoc Dunn's multiple comparisons test. Data are shown as mean ± SEM. 'n' refers to mice number. Source data are provided as a Source Data file.

mice, respectively (Fig. 7e). We quantified the number of labelled cells in the DRN/vlPAG and found that PVT-projecting and LH-projecting NPY$^{DRN/vlPAG}$ neurons exhibited different spatial pattern (Fig. 7f), indicating that the majority of NPY$^{DRN/vlPAG}$ neurons projected exclusively to either PVT or LH. Together these results showed that NPY$^{DRN/vlPAG}$ neurons actively regulate in stress-related feeding and valent behaviors via projections to the PVT and LH, respectively.

NPY$^{DRN/vlPAG}$ neurons are GABAergic neurons

To characterize the neurochemical signatures of NPY$^{DRN/vlPAG}$ neurons, we then examined the colocalization of NPY$^{DRN/vlPAG}$ neurons between several neuro-transmitter markers. We injected AAV encoding fluorescence (AAV-DIO-GFP or AAV-DIO-mCherry) into the DRN/vlPAG of *Npy$^{ires\text{-}Cre}$* mice to label NPY$^{DRN/vlPAG}$ neurons. Meanwhile, we performed FISH or immunostaining to visualize *vesicular GABA transporter (Vgat), vesicular glutamate transporter 2 (Vglut2)*, vesicular glutamate transporter 3 (VGLUT3), serotonin (5-HT) and dopamine (DA) in these viral-labeled NPY$^{DRN/vlPAG}$ neurons. The majority (~80%) of NPY$^{DRN/vlPAG}$ neurons co-express *Vgat*, with only a few (<10%) expressing *Vglut2* or VGLUT3, indicating that these NPY neurons are predominantly GABAergic (Supplementary Fig. 6c–e, h). Furthermore, there was barely any colocalization of NPY$^{DRN/vlPAG}$ neurons with 5-HT or DA (Supplementary Fig. 6f-h), indicating that NPY$^{DRN/vlPAG}$ neurons are neither serotonergic nor dopaminergic neurons.

Table 1 | Summary of NPY$^{DRN/vlPAG}$ neuronal efferent projections

Brain region	Efferent intensity
LS/MS	**
VDB/HDB	**
MPA/LPO	***
BNST	*
LH	***
AH/LA	***
PVT	**
DMH	***
PH	***
PrC	***
VTA	*
IPR	**
PAG	***
DpMe	**
CnF	***
PBN	*
LC	*
RMg	*

NPY$^{DRN/vlPAG}$ neurons project to multiple brain areas. Intensity levels of projections: * sparse; ** intermediate; *** heavy.

MS medial septal nucleus, *VDB* nucleus of the vertical limb of the diagonal band, HDB nucleus of the horizontal limb of the diagonal band, *LPO* lateral preoptic area, *BNST* bed nucleus of the stria terminalis, *PH* posterior hypothalamic area, *PrC* precommissural nucleus, *VTA* ventral tegmental area, *IPR* interpeduncular nucleus, rostral subnucleus, *DpMe* deep mesencephalic nucleus, *CnF* cuneiform nucleus, *PBN* parabrachial nuclei, *LC* locus coeruleus, *RMg* raphe magnus nucleus.

To further investigate the synaptic connectivity characteristics of NPY$^{DRN/vlPAG}$-derived projections, we performed voltage-clamp electrophysiological recordings in brain slices of NPY^{hChR2} mice. Light stimulation of NPY$^{DRN/vlPAG}$-derived projections (10 mW, 5 ms pulse) in either the PVT or the LH rapidly evoked postsynaptic currents in the presence of TTX and 4-AP (Fig. 7g, h), confirming that PVT and LH neurons received functional monosynaptic input from NPY$^{DRN/vlPAG}$ neurons. Consistent with FISH results, light-evoked postsynaptic currents were abolished by application of the GABA-A receptors blocker picrotoxin (PTX) but not the AMPA-type glutamate receptor blocker DNQX (Fig. 7g, h), indicating that the observed evoked-currents are inhibitory GABAergic in nature. Collectively, these results indicated that NPY$^{DRN/vlPAG}$ neurons provide monosynaptic inhibitory outputs to the PVT and LH.

NPY Y1 and Y2 receptors (referred to as Y1R and Y2R) are widely expressed in the LH[43], while Y2R can be observed in the PVT[44] with relatively little Y1R expression[45]. To evaluate the involvement of NPY receptor types in the PVT and LH for anti-stress effects, we employed voltage-clamp recordings in brain slices of NPY^{hChR2} mice. We found that blocking Y2R with antagonist JNJ-31020028 mainly increased the amplitude of light-evoked IPSC in the PVT (8 in 11 cells) and LH (5 cells) (Supplementary Fig. 6i, j). In contrast, Y1R receptor antagonist BIBO3304 had mild effect on the amplitude increase of light-evoked IPSC in the LH (4 in 7 cells). To conclude, Y2R plays a key role in the inhibitory effect of NPY$^{DRN/vlPAG}$ neurons in the PVT and LH, whereas Y1R in the LH may have minimal contribution.

Monosynaptic inputs to NPY$^{DRN/vlPAG}$ neurons

To gain a global perspective on the sources of inputs to NPY$^{DRN/vlPAG}$ neurons, we examined the monosynaptic inputs of these neurons using a Cre-dependent, modified rabies virus-based whole-brain tracing strategy (Supplementary Fig. 6k). We observed retrograde-labeled neurons in 34 brain regions (Table 2), and many of them, including the medial prefrontal cortex (mPFC)[46], the MPA/MPO, and the PAG[47] (Supplementary Fig. 6l), have been shown to be involved in stress responses. Further studies are needed to clarify which regions transmit stress-related signals to activate NPY$^{DRN/vlPAG}$ neurons when coping with stress.

Discussion

Stress stands as a significant contributor to both psychosocial and physical pathological conditions in humans. Identifying the neuronal

Table 2 | Summary of NPY$^{DRN/vlPAG}$ neuronal afferent projections

Brain region	Afferent intensity
MO	*
VO	*
M1	*
M2	**
S1	*
Cg1	*
PrL	***
IL	**
MPA/MPO	***
BNST	*
LGP	***
ZI	**
AuV	**
TeA	**
Ect	**
LH	***
DMH	***
pv	**
PAG	**
SC	**
PIL	*
PP	*
DpMe	**
VTA	*
PnO	*
PnC	**
PnV	*
CnF	**
RMg	**
PBN	*
LC	**
LPGi	**
Gi	*
CoP	*

NPY$^{DRN/vlPAG}$ neurons receive direct inputs from multiple brain areas. Intensity levels of projections: * sparse; ** intermediate; *** heavy.
MO medial orbital cortex, *VO* ventral orbital cortex, *M1* primary motor cortex, *M2* secondary motor cortex, *S1* primary somatosensory cortex, *Cg1* cingulate cortex, area 1, *PrL* prelimbic cortex, *IL* infralimbic cortex, *LGP* lateral globus pallidus, *ZI* zona incerta, *AuV* secondary auditory cortex, ventral area, *TeA* temporal association cortex, *Ect* ectorhinal cortex, *pv* periventricular fiber system, *SC* superior colliculus, *PIL* posterior intralaminar thalamic nucleus, *PP* peripeduncular nucleus, *PnO* pontine reticular nucleus, oral part, *PnV* pontine reticular nucleus, ventral part, *PnC* pontine reticular nucleus, caudal part, *LPGi* lateral paragigantocellular nucleus, *Gi* gigantocellular reticular nucleus, *Cop* copula of the pyramis.

mechanisms and substrates that make individuals resistant or less vulnerable to stressful stimuli is crucial for developing innovative strategies to alleviate stress-related disorders. Here, our results showed that a specific population of NPY neurons in the brainstem plays a crucial role in resisting stress-induced hypophagia and anxiety-like behaviors. Similar to the neurons mediating stress responses, *e.g.*, corticotropin-releasing hormone (CRH) neurons in the PVN[48], these NPY$^{DRN/vlPAG}$ neurons also respond quickly to various stressful stimuli marked by a rapid increase in neuronal activity. Prolonged novelty stress or stress recovery period did not continuously activate NPY$^{DRN/vlPAG}$ neurons, suggesting that they are mainly active and functional at the onset of stress. Feeding behavior decreased NPY$^{DRN/vlPAG}$ neuronal activity, suggesting a fundamental role of NPY$^{DRN/vlPAG}$ neurons in stress-induced hypophagia.

The PVN CRH neurons are inhibited by corticosterone through a negative feedback mechanism involving the HPA axis or by reward pathways, representing essential negative feedback mechanisms for stress adaptation and relief[48]. By contrast, NPY$^{DRN/vlPAG}$ neurons are activated during stress and resist stress-induced hypophagia and anxiety. Notably, NPY$^{DRN/vlPAG}$ neurons send inhibitory projections to the downstream PVT and LH regions separately, contributing to distinct anxiolytic effect in response to stress stimuli. The NPY$^{DRN/vlPAG}$ → PVT neural circuit alleviates stress-induced hypophagia, while the NPY$^{DRN/vlPAG}$ → LH neural circuit transmits positive valence. Moreover, we demonstrated that Y2R antagonist increased the amplitude of IPSC induced by light stimulation in both the PVT and LH. Y2R is a well-known NPY receptor involved in stress modulation. Previous studies have shown that Y2R antagonist BIIE0246 exerted an anxiolytic effect via intracerebroventricular injection[49], while Y2R agonist NPY13-36 produced similar anxiolytic effect when administrated into locus coeruleus (LC)[50]. Our findings suggest that Y2R plays a role in the GABA-mediated inhibitory effect by NPY$^{DRN/vlPAG}$ neurons in the PVT and LH, enhancing our understanding of brain region-specific role of Y2R in stress regulation. Overall, our study reveals a feedforward inhibition neural mechanism in regulating stress response (Supplementary Fig. 7).

Two contrasting mechanisms balance the responses to stress: one makes individuals more vigilant and vulnerable, and the other makes them more resistant or resilient. Although activated by stress, activating NPY$^{DRN/vlPAG}$ neurons resist stress rather than inducing stress-related behaviors. This is reasonable because stress must activate both stress response-eliciting neurons and stress response-resisting neurons, so that organism undergoes stress response in a proper level. Initially, stress response-eliciting neurons predominate, leading to corresponding stress response. For example, PVN→lateral septum (LS) circuits are activated by stress and elicit stress-induced hypophagia and anxiety[7,51]; Neurons in the right insular cortex (IC) can be activated by aversive stimulus and its activation causes suppressed food intake[52]. Subsequently, stress response-resisting neurons mitigate stress overactivation and facilitate the body's recovery from stress. As stress response-resisting neurons, NPY$^{DRN/vlPAG}$ neurons are activated by stressors to prevent overreactions during stress and increase food intake suppressed by stress. Therefore, when NPY$^{DRN/vlPAG}$ neurons are chemogenetically activated, they exhibit an increase in food intake as a stress-resisting effect.

On the other hand, the interaction between these two contrasting mechanisms remains unclear. Activation of NPY$^{DRN/vlPAG}$ neurons reduced the number of stress-activated Fos^{+} neurons in the PVN. However, NPY$^{DRN/vlPAG}$ neurons did not send direct projections to the PVN and manipulating NPY$^{DRN/vlPAG}$ neurons has mild effects on serum corticosterone levels. This suggests a potential indirect regulatory mechanism for NPY$^{DRN/vlPAG}$ neurons to interact with the HPA axis, possibly through the involvement of the PVT and LH. The PVT is known to integrate metabolic information to modulate feeding behavior within multiple neural circuits. Activating VGLUT2^{PVT} neurons suppresses food intake[53]. LH neurons are also activated by stress and have been involved in multiple stress-related neural circuits[54,55]. For example, orexin neurons in the LH project to the PVN[56] and activate the HPA axis to mediate stress response[57]. The close connections between the PVT and LH with the PVN indicate their potential roles in relaying signals from NPY$^{DRN/vlPAG}$ to the PVN, which may control endocrine and behavioral responses to stress. Future experiments are needed to elucidate the anatomical and functional connections among these brain areas in the regulation of stress.

We found that NPY$^{DRN/vlPAG}$ neurons are critical for resisting both stress-induced hypophagia and anxiety. As a well-known feeding stimulator[58], NPY has long been implicated in the control of feeding behavior and energy homeostasis. NPY neurons co-expressing agouti-related protein (AgRP) in the ARC stimulate feeding and promote

obesity development[27,59]. Although both inhibited by feeding behaviors, in contrast to AgRP/NPY^{ARC} neurons, NPY$^{DRN/vlPAG}$ neurons are neither sufficient nor required for maintaining ad libitum feeding or body weight homeostasis. Moreover, mice avoided activation of AgRP/NPY neurons and AgRP/NPY neuronal inhibition conditioned place preference, suggesting that AgRP/NPY neuron activity has negative valence[60]. This is in direct contrast to NPY$^{DRN/vlPAG}$ neurons that transmit a positive valence in the RTPP test.

NPY seems to be at the crossroads of stress and feeding[61]. NPY knockout mice reduced food intake after restraint stress[62]. A recent study reported that NPY neurons in the CeA stimulate high-calorie food intake and promote obesity development under chronic stress conditions[4], highlighting the role of NPY in regulating stress-induced feeding. Indeed, knocking down NPY$^{DRN/vlPAG}$ not only exacerbated acute stress-induced hypophagia, but also significantly worsened anxiety-like behaviors after stress. This is consistent with NPY's anxiolytic properties. In contrast to chemogenetic inhibition of NPY$^{DRN/vlPAG}$ neurons, knocking down NPY$^{DRN/vlPAG}$ did not impact chronic restraint stress-induced body weight reductions. This suggests that other molecules, possibly GABA, might have roles in counteracting the reductions in food intake and body weight induced by chronic restraint stress. In fact, a previous study has shown that VGAT^{DRN} neurons stimulate food intake[63], suggesting the potential involvement of GABA in NPY$^{DRN/vlPAG}$ neurons in mitigating chronic stress-induced hypophagia. Further explorations are needed to differentiate the functional differences and target actions between NPY and GABA in NPY$^{DRN/vlPAG}$ neurons.

Together, our findings identified a population of previously uncharacterized anxiolytic NPY neurons that play a significant role in ameliorating anorexia and anxiety during stress. Understanding the circuitry involved in stress resistance will guide the future development of therapeutic strategies for stress-related disorders.

This study has several limitations that need to be addressed in future research. Firstly, behavioral experiments were only conducted in male mice, and both male and female mice were used in several immunostaining experiments. Stress activates typical neuronal circuits, such as the HPA axis and sympathetic nervous system, in both sexes. However, it has been suggested that males and females sometimes exhibit distinct stress responses[64]. Thus, it is possible that NPY$^{DRN/vlPAG}$ neurons exhibit sex-specific differences in regulating stress responses, which requires further investigations.

Secondly, while we observed that manipulation of NPY$^{DRN/vlPAG}$ neurons influenced the behavioral performance of animals in the OFT, it did not have the same effect in the EPM. It is worth noting that although both the OFT and EPM are commonly used paradigms to assess anxiety levels in rodents, they are influenced by different factors and reflects different aspects of stress and anxiety. This could account for the observed variations between the two paradigms in our study.

In the NPY knockdown experiments, mice were group-housed to minimize unnecessary stress. In this circumstance, average daily food intake was determined by dividing the overall food intake per cage by the number of mice. However, there were instances where one or two mice within a cage exhibited insufficient NPY$^{DRN/vlPAG}$ knockdown efficiency, which could lead to misleading data on daily food intake. Consequently, this data was not displayed.

Regarding the studies of NPY receptors, while we found that NPY from NPY$^{DRN/vlPAG}$ neurons exerts an anti-stress effect, these neurons project inhibitory signals to the downstream regions. However, this inhibitory effect could also be suppressed by NPY. This seemingly contradiction requires further investigations, potentially involving specific microcircuit mechanisms.

Finally, we employed various methods to activate and inhibit NPY$^{DRN/vlPAG}$ neurons, which could introduce some variability. To mitigate this concern, we validated the specificity and efficacy of our targeting and manipulation techniques through electrophysiological recording, immunostaining, and FISH techniques. Additionally, chemogenetic experiments using CNO and its metabolite clozapine present potential limitations[37], both of which were employed in this study. Control mice expressing only fluorescence were included to address off-target effects. However, receptor desensitization remains a potential issue following several days of CNO/clozapine injection[65]. AAV-mediated delivery can offer persistent and overexpression of receptors to counteract such desensitization[65], and the changes in food intake in our study were observed early during the CNO/clozapine injection period, likely before desensitization occurred. Overall, while chemogenetic manipulation may reduce efficacy, it is unlikely to significantly impact our conclusions.

Methods

Mice

All animal experimental procedures were conducted following protocols approved by institutional guidelines for the animal care and use of the University of Science and Technology of China (USTC) and National Institute of Biological Sciences, Beijing. *Npy$^{ires\text{-}Cre}$* mice (JAX: 027851), *Npy^{GFP}* mice (JAX: 006417), and *Rosa26^{Ai14}* mice (JAX: 007908) were all obtained from Jackson Laboratory. *Npy$^{ires\text{-}Cre}$* and *Rosa26^{Ai14}* mice were crossed to generate *Npy$^{ires\text{-}Cre}$:: Rosa26^{Ai14}* mice. *Npy$^{lox/lox}$* mice were generated and kindly provided by Herzog Herbert's lab[4]. C57BL/6 J mice were purchased from Beijing Vital River Laboratory. All transgenic mice used in this study were backcrossed to the C57BL/6 J background. All experiments were performed on adult mice (8-16 weeks old). Male mice were used for behavior and physiology studies to avoid sex variation derived from hormone, while both male and female mice were used for immunostaining studies. Mice were housed in a controlled environment with a 22-25 °C temperature and 12-h light/dark cycle (light on at 7 a.m.). Standard chow (SPF rodent diet, SPF (Beijing) Biotechnology Co., Ltd., China) and water were provided ad libitum.

AAV virus

For chemogenetic studies, AAV9-hSyn-DIO-hM3D(Gq)-mCherry (Addgene, 44361-AAV9, 2E + 12 V.G/ml) and AAV2/9-hSyn-DIO-hM4D(Gi)-eGFP-WPRE-pA (Taitool, S0286-9, 2.5E + 12 V.G/ml) were used. For optogenetic studies, AAV9-EF1a-DIO-hChR2(H134R)-mCherry-WPRE-HGH-pA (Addgene, 20297-AAV9, 2.8E + 12 V.G/ml) and AAV2/9-hSyn-DIO-hGtACR1-EGFP-WPRE-pA (Taitool, S0575-9, 2.5E + 12 V.G/ml) were used. For anterograde tracing studies, AAV2/9-hSyn-FLEX-mGFP-2A-Synaptophysin-mRuby-WPRE-pA (Taitool, S0250-9, 2E + 12 V.G/ml) were used. For retrograde tracing studies, rAAV-Ef1α-DIO-TVA-P2A-NLS-dTomato-WPRE-hGH-pA (BrainVTA, PT-0149, 5.15E + 12 V.G/ml), rAAV-EF1α-DIO-RVG-WPRE-hGH-pA (BrainVTA, PT-0023, 3.4E + 12 V.G/ml), RV-CVS-ENVA-N2C(ΔG)-EGFP (BrainVTA, R05001, 2.8E + 8 IFU/ml), AAV2/2Retro Plus-hSyn-FLEX-m_tdTomato-WPRE-pA (Taitool, S0330-2RP, 1E + 13 V.G/ml) and AAVrg-hSyn-DIO-EGFP (Addgene, 50457-AAVrg, 1E + 13 V.G/ml) were used. For the control groups, AAV2/9-hSyn-DIO-mCherry-WPRE-pA (Taitool, S0240-9, 1E + 12 V.G/ml), AAV2/5-hSyn-DIO-mGFP (Taitool, S0276-5, 1E + 12 V.G/ml) and AAV9-hSyn-mCherry-WPRE-pA (Taitool, S0238-9, 1E + 12 V.G/ml) were used. Other viruses used in the studies included AAV2/9-CAG-DIO-taCaspase3-TEVp-WPRE-pA (Taitool, S0236-9, 3.3E + 12 V.G/ml), AAV9-hSyn-Cre-EGFP-WPRE-pA (Taitool, S03230-9, 3E + 12 V.G/ml) and AAV9-Syn-Flex-GCaMP6m-WPRE-SV40 (Addgene, 100838-AAV9, 2.2E + 12 V.G/ml).

Stereotaxic surgery

Mice were anesthetized with 2,2,2-tribromoethanol (i.p., Sigma-Aldrich, T48402, 250 mg/kg) dissolved in 2.5% 2-methyl-2-butanol and placed in a stereotaxic holder (RWD Life Science, China). Eyes were covered with an eye ointment. A heating pad was provided to maintain the animals' body temperature. After exposure of the skull, a small hole was carefully opened to avoid bleeding. Virus was infused into the

targeted brain region at a speed of 40 nl/min (Nanoliter 2000 Injector, WPI). All mice were allowed to recover for at least two weeks before any further experiments.

For chemogenetic experiments, AAV9-hSyn-DIO-hM3D(Gq)-mCherry (180 nl for each side) or AAV2/9-hSyn-DIO-hM4D(Gi)-eGFP-WPRE-pA (220 nl for each side) were bilaterally injected into the DRN/vlPAG region (coordinate: anterior-posterior (AP) -3.85 mm, medial-lateral (ML) ± 0.2 mm, dorsal-ventral (DV) -2.9 mm, 15° from anterior to posterior) of Cre mice. AAV2/9-hSyn-DIO-mCherry-WPRE-pA (150 nl for each side) or AAV2/5-hSyn-DIO-mGFP (150 nl for each side) were injected into the DRN/vlPAG region as controls.

For optogenetic experiments, AAV9-EF1a-DIO-hChR2(H134R)-mCherry-WPRE-HGH-pA (180 nl for each side) and AAV2/9-hSyn-DIO-hGtACR1-EGFP-WPRE-pA (220 nl for each side) were bilaterally injected into the DRN/vlPAG region. After virus injection, one optical fiber was inserted unilaterally above the virus injection site for optogenetic activation, and two optical fibers were implanted bilaterally above the virus injection site for optogenetic inhibition. For terminal stimulation, optical fibers were inserted above the MPA/LPO (coordinate: AP 0.1 mm, ML 0.25 mm, DV −4.5 mm), PVT (coordinate: AP −0.9 mm, ML 0 mm, DV −2.7 mm), LH (coordinate: AP −0.9 mm, ML 1.1 mm, DV −4.4 mm), AH/LA (coordinate: AP −0.9 mm, ML 0.4 mm, DV -4.6 mm) or DMH (coordinate: AP −1.8 mm, ML 0.35 mm, DV −4.55 mm), respectively. AAV2/9-hSyn-DIO-mCherry-WPRE-pA (150 nl for each side) was injected into the DRN/vlPAG region as controls. Optical fiber cannulas were fixed with dental cement.

For fiber photometry recording experiments, AAV9-Syn-Flex-GCaMP6m-WPRE-SV40 (150 nl for each side) was bilaterally injected into the DRN/vlPAG region of Cre mice. AAV2/5-hSyn-DIO-mGFP (150 nl for each side) was injected into the DRN/vlPAG region of Cre mice as controls. After virus injection, one optical fiber was implanted unilaterally above the virus injection site with dental cement.

For neuron ablation studies, AAV2/9-CAG-DIO-taCaspase3-TEUp-WPRE-pA (600 nl for each side) was bilaterally injected into the DRN/vlPAG region of *Npy*$^{ires\text{-}Cre}$*::* *Rosa26*^{Ai14} mice. AAV2/9-CAG-DIO-taCaspase3-TEUp-WPRE-pA was injected bilaterally into the DRN/vlPAG region of *Npy*$^{+/+}$*::* *Rosa26*^{Ai14}mice as controls.

For NPY knockdown experiment, AAV9-hSyn-Cre-EGFP-WPRE-pA (300 nl for each side) was bilaterally injected into DRN/vlPAG of *Npy*$^{lox/lox}$ mice. AAV9-hSyn-mCherry-WPRE-pA (150 nl for each side) was bilaterally injected into DRN/vlPAG of *Npy*$^{lox/lox}$ mice as controls.

For the anterograde tracing experiment, AAV2/9-hSyn-FLEX-mGFP-2A-Synaptophysin-mRuby-WPRE-pA (180 nl for each side) was bilaterally injected into the DRN/vlPAG of Cre mice.

For retrograde non-transsynaptic tracing experiment, AAV2/2Retro Plus-hSyn-FLEX-m_tdTomato-WPRE-pA (50 nl for each side) was bilaterally injected into the LH and AAVrg-hSyn-DIO-EGFP (100 nl) was injected into the PVT of Cre mice.

For retrograde transsynaptic tracing experiment, a mixture of rAAV-Ef1α-DIO-TVA-P2A-NLS-dTomato-WPRE-hGH-pA and rAAV-EF1α-DIO-RVG-WPRE-hGH-pA (1:1, 300 nl for each side) were bilaterally injected into DRN/vlPAG of Cre mice. Two weeks later, RV-CVS-ENVA-N2C(ΔG)-EGFP (70 nl for one side) was bilaterally injected into the same region. Mice were sacrificed after 10-day expression of RV virus.

Immunofluorescence

Mice were anesthetized with 2,2,2-tribromoethanol (i.p., Sigma-Aldrich, T48402, 250 mg/kg) dissolved in 2.5% 2-methyl-2-butanol. After anesthesia, mice were perfused with cold saline and then 4% paraformaldehyde (PFA, Aladdin, C104188, in PBS) to fix the brain. Brains were extracted and postfixed in 4% PFA overnight and then dehydrated with 30% sucrose. Dehydrated brains were cut coronally into 50-μm sections. For immunostaining experiments, the brain sections were washed with PBST (0.3% Triton X-100, in PBS) three times and incubated with blocking buffer (3% BSA, in PBST) for 1 h. These brain sections were then incubated with the indicated primary antibodies at 4 °C overnight. On the following day, brain sections were washed with PBST three times and incubated with specific secondary antibodies for 4 hs at room temperature. Following another round of 3 times of washing, brain sections were mounted and covered with DAPI (MCE, HY-D0814, 4 μg/ml) for further examination under microscopes.

The primary antibodies used were as follows: chicken anti-mCherry (Abcam, ab205402, 1:500), chicken anti-GFP (Abcam, ab13970, 1:1000), rabbit anti-c-Fos (Cell Signaling Technology, 2250, 1:1000), rabbit anti-NPY (Abcam, ab30914, 1:1000), rabbit anti-VGLUT3 (Synaptic Systems, 135203, 1:500), rabbit anti-5-HT (ImmunoStar, 20080, 1:500) and rabbit anti-Tyrosine Hydroxylase (Merck Millipore, AB152, 1:1000). Secondary antibodies included goat-anti-rabbit-647 (Jackson ImmunoResearch, 111-605-003, 1:1000), goat-anti-rabbit-488 (Jackson ImmunoResearch, 111-545-003, 1:1000), goat-anti-chicken-488 (Thermo Fisher, A11039, 1:1000) and donkey-anti-chicken-cy3 (Jackson ImmunoResearch, 703-165-155, 1:1000).

RNA fluorescence in situ hybridization (FISH)

After anesthetized with 2,2,2-tribromoethanol (i.p., Sigma-Aldrich, T48402, 250 mg/kg) dissolved in 2.5% 2-methyl-2-butanol, mice were perfused with cold 0.01 M DEPC (Sigma-Aldrich, D5758) -treated saline (DEPC-saline) and then 4% PFA (in DEPC-PBS) to fix the brain. The brains were extracted into 4% PFA (in DEPC-PBS) overnight for further fixation and then moved to 30% sucrose for dehydration. The dehydrated brains were cut coronally into 40-μm slices and collected in DEPC-PBS followed with the following FISH protocol[66]: In short, brain slices were washed with DEPC-PBS, permeabilized with DEPC-PTW (0.1% Tween20 in DEPC-PBS) and 0.5% Triton in 2 × SSC, and went through acetylation and 3% hydrogen peroxide (in methanol) to reduce background noise. After a 2-h incubation with prehybridization buffer (50% formamide, 5 × SSC, 0.1% Tween20, 0.1% CHAPS, 5 mM EDTA pH 8.0), brain slices were hybridized at 65 °C in the hybridization solution (50% formamide, 5 x SSC, 0.1 mg/ml Heparin, 1 x Denhalt's solution, 0.1% Tween20, 5 mM EDTA, 0.3 mg/ml tRNA, 0.1% CHAPS) for 20 hs with 500 ng/ml digoxigenin-labeled antisense cRNA probes. When the hybridization was finished, brain slices were washed with TBST and incubated 30 hs with Anti-Digoxigenin-POD (Roche, 11207733910, 1:500) at 4°C. Finally, brain slices were incubated with TSA Plus kits (PerkinElmer, NEL741001KT for Fluorescein, NEL744001KT for Cyanine 3 and NEL745B001KT for Cyanine 5, 1:100) to visualize probes. Since initial fluorescent signals were quenched because of 65 °C environment, brain slices were then incubated with corresponding antibodies for signal recovery (following the instruction of "Immunofluorescence" above). The primers used to amplify antisense cRNA probes were as follows: *Vgat* (5′-GCCATTCAGGGCATGTTC and 5′-AGCAGCGTGAAGACCACC, probe 952 bp), *Vglut2* (5′-CCAAATCTTACGGTGCTACCTC and 5′-TAGCCATCTTTCCTGTTCCACT, probe 580 bp) and *Npy* (5′-CGCCACGATGCTAGGTAACAA and 5′-CACCACATGGAAGGGTCTTCA, probe 300 bp).

Whole-cell patch-clamp electrophysiological recordings

Mice were anesthetized with isoflurane and then decapitated. The brain was quickly extracted and sliced coronally at a thickness of 250 μm with a Leica VT1200S Vibratome slicer (Leica, Germany) in ice-cold N-methyl-D-glucamine (NMDG) cutting solution saturated with 95% O_2/5% CO_2. The NMDG solution comprised 92 mM NMDG, 1.2 mM KCl, 30 mM $NaHCO_3$, 1.2 mM KH_2PO_4, 25 mM D-Glucose, 20 mM HEPES, 5 mM L-ascorbic acid, 3 mM Na-pyruvate, 2 mM thiourea, 10 mM $MgSO_4$, and 0.5 mM $CaCl_2$ with an osmolarity of 310 ± 5 mOsm/L and a pH of 7.2 ± 0.1. The brain slices were then incubated in artificial cerebrospinal fluid (ACSF) saturated with 95% O_2/5% CO_2 at 37 °C for at least 45 min and allowed to recover for about 1 h at room temperature before recording. The ACSF solution contained 125 mM NaCl, 1.25 mM KCl, 25 mM $NaHCO_3$, 1.25 mM KH_2PO_4, 25 mM D-Glucose, 0.4 mM L-ascorbic acid, 2 mM Na-pyruvate, 2 mM $CaCl_2$ and 1 mM $MgCl_2$.

After recovery, the brain slices were placed in the recording chamber and continuously perfused with ACSF at 1–2 ml/min. Brain sections were observed under an Olympus BX51WI microscope with infrared (IR)-differential interference contrast (DIC) and a charge-coupled device (CCD) camera (IR-2000; DAGE-MTI). Patch pipettes were pulled from borosilicate glass capillary tubes (OD = 1.5 mm, ID = 0.84 mm, Sutter Instrument) to achieve a final tip resistance of 4-7 MΩ by a puller (Model P-1000, Sutter Instrument).

For action potentials (current clamp) recording, the internal solution contained 26 mM K-gluconate, 10 mM Hepes, 4 mM KCl, 4 mM Mg-adenosine triphosphate (ATP), 0.3 mM Na4-guanosine triphosphate (GTP) and 10 mM phosphocreatine. For postsynaptic currents (voltage clamp) recording, the internal solution contained 40 mM CsCl, 3.5 mM KCl, 10 mM HEPES, 0.05 mM EGTA, 90 mM K-gluconate, 1.8 mM NaCl, 1.7 mM MgCl2, 2 mM ATP, 0.4 mM GTP, 10 mM phosphocreatine and 5 mM QX-314.

For chemogenetic validation, CNO (ENZO, BML-NS105-0025, 10 μM for hM3Dq activation and 50 μM for hM4Di inhibition) or clozapine (MCE, HY-14539, 5 μM for hM4Di inhibition) were dissolved in ACSF and perfused to brain slices. Basal frequency of action potential and membrane potential were defined as the average frequency and membrane potential obtained 3 mins before CNO or clozapine administration, while post-application frequency of action potential and membrane potential were the average obtained 5 mins after drug perfusion[67].

For optogenetic stimulation, blue light pulses (470 nm) from a LED were applied to brain sections through an Olympus 40× water-immersion lens. To record light-evoked postsynaptic currents in projection regions, hChR2-mCherry-positive nerve terminals were triggered by a single light-pulse (10 mW, 5 ms) in the presence of 4-aminopyridine (4-AP, Sigma-Aldrich, 275875, 100 μM) and tetrodotoxin (TTX, KangTe Biotechnology Co., Ltd, 201206, 1 μM). To confirm the cell type of $NPY^{DRN/vlPAG}$ neurons, DNQX (MCE, HY-15067, 20 μM) or DNQX plus PTX (MCE, HY-101391, 100 μM) were perfused with ACSF during light-evoked postsynaptic currents recording. To determine the involvement of NPY receptors in the PVT and LH, Y1R receptor antagonist BIBO3304 (MCE, HY-107725, 5 μM) or Y2R receptor antagonist JNJ-31020028 (MCE, HY-14450, 5 μM) was bath-applied. Light-evoked postsynaptic currents were recorded before and 10 mins after NPY receptors perfusion. The recorded postsynaptic currents were averaged from 8 sweeps of recording with 5-s inter-sweep-interval. All recordings were performed using an EPC 10 USB amplifier (HEKA Elektronik), and the electrophysiological data were filtered at 2.9 kHz and sampled at 20 kHz by PatchMashter 1.4.1 software.

Optogenetic and chemogenetic experiments

For chemogenetic manipulations (except for manipulations during restraint stress), mice received injections of CNO (i.p., 2 mg/kg, ENZO, BML-NS105-0025) or an equal volume of saline half an hour prior to experiments. During restraint stress, chemogenetic manipulation was performed by administering daily clozapine (i.p., 0.2 mg/kg, MCE, HY-14539) or an equal volume of saline half an hour before the onset of restraint stress.

For optogenetic activation of hChR2-expressed soma, the stimulation program was as follows: 473 nm, 10 ms pulse duration, 5 or 10 or 20 Hz frequency, 1-s on and 1-s off pattern and 10 mW optical power. For optogenetic inhibition, a continuous laser (473 nm, 3 mW optical power) was applied throughout the entire stimulation period.

For optogenetic activation of hChR2-expressed terminals, 473 nm, 10 ms pulse duration, 20 Hz frequency, 1-s on and 1-s off pattern and 10 mW optical power was employed.

Behavioral experiments

All behavioral experiments were conducted during the active period of mice. Mice were transferred to a behavior testing room several days before behavioral experiments for adaptation and kept in that room throughout behavioral experiments.

Acute novelty stress

To induce acute novelty stress, we transferred group-housed mice individually into a single-housed new cage without padding for 24 hs. Mice were provided with ad libitum access to water and a standard chow diet. Behavior tests and Fos immunostaining studies were performed after 2-h acute novelty stress, while serum collection was performed after 1-h acute novelty stress. Mice received CNO or saline injections half an hour prior to a novelty stress challenge.

Chronic restraint stress

Group-housed mice were confined in a triangular plastic bag that limited their mobility for 2–3 hs each day, and this was repeated for 14 consecutive days. A hole was created in the bag to allow the mice to breathe during restraint. Fos immunostaining studies were performed after 2-h restraint. For chemogenetic manipulations during the restraint stress, the mice were administered daily intraperitoneal injections of clozapine half an hour prior to restraint stress for a period of 14 days. Serum was collected before and after day 1 and day 14's restraint during 14-day restraint stress.

Real-time place preference test (RTPP)

A custom-made box with a two-sided chamber (L × W × H: 30 cm × 60 cm × 30 cm) was used for the RTPP test. This behavior test consisted of a 15-min pre-stimulation session, a 15-min stimulation session and a 15-min post-stimulation session. Mice were allowed to move freely in the RTPP chamber. During the stimulation phase, laser (473 nm, 10 mW, 20 Hz, 10 ms pulse, 1-s on and 1-s off for activation; 3 mW for inhibition) was turned on once the mouse traveled to the laser-paired side and was kept on when it stayed on the side. The laser was turned off when mice traveled to the non- laser-paired side. The locomotion traces were recorded with an overhead camera, and place preference was analyzed using MATLAB[68].

Open field test (OFT)

OFT was performed after the end of acute novelty stress or 14-day restraint stress. A custom-made square box (L × W × H: 48 cm × 48 cm × 48 cm) was used for the OFT. The center area (24 cm × 24 cm) was marked with black tape. Mice were allowed to move freely in the OFT for 10 mins. The locomotion traces were recorded with an overhead camera and were analyzed using MATLAB[68].

Elevated plus maze test (EPM)

EPM was performed after the end of acute novelty stress or 14-day restraint stress. A plus maze with two closed and two open arms (L × W: 24.5 cm × 6 cm) was used for the EPM. The maze was placed on a shelf 45 cm above the ground. Mice were placed in the center of the maze at the onset of the experiment and allowed to move freely in the EPM for 5 mins. The locomotion traces were recorded with an overhead camera and were analyzed using MATLAB[68].

Measurement of food intake and body weight

Food intake and body weight were manually measured. We carefully checked for any remaining food pellets in cages when the experiments were completed, and in most cases, there are no food leftovers. To minimize the chance of food pellets falling into the cage, we used larger food pellets whenever possible. When weighing the food, we handled it very carefully to minimize any disturbances to the animals. In the fasting-refeeding study, food was removed from mice cages for 16 hs. In all stress models, food intake of group-housed mice was calculated by dividing the total amount of food in each cage by the number of mice in the cage. In the acute novelty stress model with chemogenetic manipulation, food intake was measured at 1, 2, 3, 4, and 24-h after the onset of stress. In the acute novelty stress model

with optogenetic manipulation, food intake was measured 1 and 2-h after the onset of stress. In the chronic restraint stress model, body weight and 24-h food intake were measured once daily.

Measurement of serum corticosterone levels

In the acute novelty stress model, 1 h after novelty stress, the end of the mouse tail was gently cut, and ~5 μl of blood was drawn into a tube. In the chronic stress model, the same blood collection approach was used before and after day 1 and day 14's restraint during 14-day restraint stress. The serum was then collected by centrifugation (1000 *g*, 15 min, 4 °C), and a commercial ELISA kit (ENZO, ADI-900-097) was used to measure serum corticosterone levels according to the manufacturer's instructions.

Fiber photometry recording

A fiber photometry system was used for in vivo recording of neuronal calcium signals[69] (BiolinkOptics, Beijing). Briefly, a dichroic mirror (MD498, Thorlabs) was utilized to reflect 488 nm excitation light from a laser (OBIS 488LS, Coherent). Excitation light from the laser and emission fluorescent signals from the mouse brain were all delivered through an optical fiber (200 μm diameter, 0.39 NA, 2 m long, Thorlabs). The fluorescence signals were collected with a photomultiplier tube (R3896, Hamamatsu) and filtered by a bandpass filter (MF525-39; Thorlabs) and a low-pass filter (40 Hz, Brownlee 440). The laser power at the fiber tip was ~30 μW. Sample read frequency was 100 Hz for all recording experiments except for 10-min acute novelty stress test, whose sample read was 10 Hz.

All fiber photometry recording experiments were conducted in the dark phase except for fasting-refeeding experiment (in the light phase). In the fasting-refeeding test, mice were fasted for 16 hs overnight. On the next day, mice were connected to fiber photometry device and food was provided into the cage. The entire recording lasted about 45 mins. In the tail suspension test, mice were suspended by their tails 30 cm above ground for ~3 s and then returned to their home cages. The test was repeated for 5–10 trials for each mouse. In the novelty object contact test, a novel plastic object was put in the cage and the time point when mice made contact with the novel object in the first 5 mins were recorded. In the restraint test, mice were manually held by the experimenter's hands for 5 s, which was repeated for 7–11 trials for each mouse.

In the acute novelty stress paradigm, a group-housed mouse was connected to a fiber photometry device in its home cage and then transferred to a new cage without padding. The mouse was allowed to move freely in the new cage for 1 or 10 mins and then returned to its home cage. During the course of this experiment, in order to prevent other animals from escaping, the other mice in the same home cage were temporarily transferred to another cage. The 1-min test was repeated for 4-8 trials for each mouse. Additionally, the time point of grooming and standing up during acute novelty stress were also recorded for further statistics.

In the chronic novelty stress test, a group-housed mouse was connected to a fiber photometry device for the following recording. The mouse was allowed to move freely in the home cage for 30 mins, then transferred to a new cage without padding for 4 hs, finally transferred back to the home cage for another 30 mins. During the whole 5-h recording, 1-min fluorescence signal was collected every 10 mins, and the average fluorescence of the last 50 s within 1-min period was defined as the fluorescence intensity value for that 10-min time point.

Fluorescence change (ΔF/F) was determined by calculating (F − F0)/(F0 − Fb), where Fb is the background noise of the fiber photometry device. F0 is the average fluorescence signal of −5 to −2 s of each recording for acute stress-related tests, and −6 to −4 s of each food bite in fasting-refeeding test. In the chronic novelty stress, F0 is the average fluorescence intensity of the first 30 min. The fluorescence change for one mouse in every test is defined as the average of all trails in this test.

Imaging analysis

Brain slices images were acquired using an automated scanner (Olympus, VS120) or a confocal microscope (Nikon, A1 and Olympus, SpinSR) and visualized by software OlyVIA 4.1 or NIS elements 5.20.00 to validate viral/protein expression or fiber positions. To count the number of Fos/NPY-positive neurons, we collected all or one in every two brain slices. Specific brain regions were identified according to the Paxinos & Franklin mouse brain atlas, and cell numbers were counted using ImageJ 1.53t software. The cell number with co-expression of two different fluorescence was manually counted.

To measure NPY fluorescent intensity in NPY knockdown experiment, NPY expression regions (target) and their nearby regions without fluorescence (background) were outlined. Area, integrated density and mean grey value were all measured for each region by ImageJ software. NPY fluorescent intensity = target region integrated fluorescent density − area of target region × mean grey value of background region. $NPY^{DRN/VLPAG}$ expression for one mouse was defined as the average of all $NPY^{DRN/VLPAG}$ fluorescent intensity.

Statistical analysis

All data points are taken from distinct samples. Statistical analyses were performed using GraphPad Prism 9.3.1 and MATLAB R2020a. Two-group unpaired comparisons with one factor were analyzed using two-sided unpaired Student's *t* test for data with a normal distribution or two-sided Mann Whitney test for data without a normal distribution; Two-sided unpaired Student's *t* test with Welch's correction was used for data with a normal distribution but heterogeneous variance. Two-group paired comparisons with one factor were analyzed using two-sided paired Student's *t* test for data with a normal distribution or two-sided Wilcoxon matched-pairs signed rank test for data without a normal distribution.

Three-group unpaired comparisons with one factor were analyzed using ordinary one-way ANOVA for data with a normal distribution, with post-hoc Dunnett's multiple comparisons test. For data without a normal distribution, Kruskal-Wallis test was used with post-hoc Dunn's multiple comparisons test.

Three-group paired comparisons with one factor were analyzed using Repeated measures one-way ANOVA for data with a normal distribution, with post-hoc Tukey's multiple comparisons test. For data without a normal distribution, two-sided Friedman test was used with post-hoc Dunn's multiple comparisons test.

Comparisons between groups with two factors were analyzed using two-way repeated-measures ANOVA, with post-hoc Šídák's or Tukey's multiple comparisons test.

Statistical details, including animal numbers, p values, and statistical test types, are described in the figures or figure legends. All data are shown as the means ± SEM. $p < 0.05$ was considered significant.

Reporting summary

Further information on research design is available in the Nature Portfolio Reporting Summary linked to this article.

Data availability

All data generated in this study are provided within the article, Supplementary Information and Source Data file. Further information regarding to the findings in the present study are available from the corresponding authors upon request. Source data are provided with this paper.

Code availability

Custom made codes for photometry data export and animal route tracking are available from the corresponding authors upon request.

References

1. Hirsch, D. & Zukowska, Z. NPY and stress 30 years later: the peripheral view. *Cell Mol. Neurobiol.* **32**, 645–659 (2012).
2. Daviu, N., Bruchas, M. R., Moghaddam, B., Sandi, C. & Beyeler, A. Neurobiological links between stress and anxiety. *Neurobiol. Stress* **11**, 100191 (2019).
3. Yang, L. et al. The effects of psychological stress on depression. *Curr. Neuropharmacol.* **13**, 494–504 (2015).
4. Ip, C. K. et al. Amygdala NPY circuits promote the development of accelerated obesity under chronic stress conditions. *Cell Metab.* **30**, 111–128 (2019).
5. Maniam, J. & Morris, M. J. The link between stress and feeding behaviour. *Neuropharmacology* **63**, 97–110 (2012).
6. Yehuda, R. Post-traumatic stress disorder. *N. Engl. J. Med.* **346**, 108–114 (2002).
7. Xu, Y. Z. et al. Identification of a neurocircuit underlying regulation of feeding by stress-related emotional responses. *Nat. Commun.* **10**, 3446 (2019).
8. Albrecht, A., Redavide, E., Regev-Tsur, S., Stork, O. & Richter-Levin, G. Hippocampal GABAergic interneurons and their co-localized neuropeptides in stress vulnerability and resilience. *Neurosci. Biobehav. Rev.* **122**, 229–244 (2021).
9. Edvinsson, L., Ekblad, E., Håkanson, R. & Wahlestedt, C. Neuropeptide Y potentiates the effect of various vasoconstrictor agents on rabbit blood vessels. *Br. J. Pharmacol.* **83**, 519–525 (1984).
10. Zhang, L., Bijker, M. S. & Herzog, H. The neuropeptide Y system: pathophysiological and therapeutic implications in obesity and cancer. *Pharmacol. Ther.* **131**, 91–113 (2011).
11. Levine, A. S. & Morley, J. E. Neuropeptide Y: a potent inducer of consummatory behavior in rats. *Peptides* **5**, 1025–1029 (1984).
12. Reichmann, F. & Holzer, P. Neuropeptide Y: a stressful review. *Neuropeptides* **55**, 99–109 (2016).
13. Heilig, M., Söderpalm, B., Engel, J. A. & Widerlöv, E. Centrally administered neuropeptide Y (NPY) produces anxiolytic-like effects in animal anxiety models. *Psychopharmacology* **98**, 524–529 (1989).
14. Kask, A. et al. The neurocircuitry and receptor subtypes mediating anxiolytic-like effects of neuropeptide Y. *Neurosci. Biobehav. Rev.* **26**, 259–283 (2002).
15. Cohen, H. et al. The neuropeptide Y (NPY)-ergic system is associated with behavioral resilience to stress exposure in an animal model of post-traumatic stress disorder. *Neuropsychopharmacology* **37**, 350–363 (2012).
16. Bannon, A. W. et al. Behavioral characterization of neuropeptide Y knockout mice. *Brain Res.* **868**, 79–87 (2000).
17. Sah, R., Ekhator, N. N., Jefferson-Wilson, L., Horn, P. S. & Geracioti, T. D. Jr. Cerebrospinal fluid neuropeptide Y in combat veterans with and without posttraumatic stress disorder. *Psychoneuroendocrinology* **40**, 277–283 (2014).
18. Sabban, E. L., Alaluf, L. G. & Serova, L. I. Potential of neuropeptide Y for preventing or treating post-traumatic stress disorder. *Neuropeptides* **56**, 19–24 (2016).
19. Adrian, T. E. et al. Neuropeptide Y distribution in human brain. *Nature* **306**, 584–586 (1983).
20. Hundahl, C. et al. Hypothalamic hormone-sensitive lipase regulates appetite and energy homeostasis. *Mol. Metab.* **47**, 101174 (2021).
21. Zhang, G. W. et al. Medial preoptic area antagonistically mediates stress-induced anxiety and parental behavior. *Nat. Neurosci.* **24**, 516–528 (2021).
22. Spencer, S. J., Fox, J. C. & Day, T. A. Thalamic paraventricular nucleus lesions facilitate central amygdala neuronal responses to acute psychological stress. *Brain Res.* **997**, 234–237 (2004).
23. Leistner, C. & Menke, A. Hypothalamic-pituitary-adrenal axis and stress. *Handb Clin Neurol.* **175**, 55–64 (2020).
24. Tovote, P., Fadok, J. P. & Luthi, A. Neuronal circuits for fear and anxiety. *Nat. Rev. Neurosci.* **16**, 317–331 (2015).
25. Song, C., Berridge, K. C. & Kalueff, A. V. Stressing' rodent self-grooming for neuroscience research. *Nat. Rev. Neurosci* **17**, 591 (2016).
26. Armbruster, B. N., Li, X., Pausch, M. H., Herlitze, S. & Roth, B. L. Evolving the lock to fit the key to create a family of G protein-coupled receptors potently activated by an inert ligand. *Proc. Natl Acad. Sci. USA* **104**, 5163–5168 (2007).
27. Aponte, Y., Atasoy, D. & Sternson, S. M. AGRP neurons are sufficient to orchestrate feeding behavior rapidly and without training. *Nat. Neurosci.* **14**, 351–355 (2011).
28. Chen, J. et al. A vagal-NTS neural pathway that stimulates feeding. *Curr. Biol.* **30**, 3986–3998 (2020).
29. Yang, C. F. et al. Sexually dimorphic neurons in the ventromedial hypothalamus govern mating in both sexes and aggression in males. *Cell* **153**, 896–909 (2013).
30. Guidi, J., Lucente, M., Sonino, N. & Fava, G. A. Allostatic load and its impact on health: a systematic review. *Psychother. Psychosom.* **90**, 11–27 (2021).
31. Jeong, J. Y., Lee, D. H. & Kang, S. S. Effects of chronic restraint stress on body weight, food intake, and hypothalamic gene expressions in mice. *Endocrinol. Metab.* **28**, 288–296 (2013).
32. Liu, W. Z. et al. Identification of a prefrontal cortex-to-amygdala pathway for chronic stress-induced anxiety. *Nat. Commun.* **11**, 2221 (2020).
33. Yang, Y. et al. Ketamine blocks bursting in the lateral habenula to rapidly relieve depression. *Nature* **554**, 317–322 (2018).
34. Qu, N. et al. A POMC-originated circuit regulates stress-induced hypophagia, depression, and anhedonia. *Mol. Psychiatry* **25**, 1006–1021 (2020).
35. Haleem, D. J. Adaptation to repeated restraint stress in rats: failure of ethanol-treated rats to adapt in the stress schedule. *Alcohol Alcohol.* **31**, 471–477 (1996).
36. Patel, S. & Hillard, C. J. Adaptations in endocannabinoid signaling in response to repeated homotypic stress: a novel mechanism for stress habituation. *Eur. J. Neurosci.* **27**, 2821–2829 (2008).
37. Gomez, J. L. et al. Chemogenetics revealed: DREADD occupancy and activation via converted clozapine. *Science* **357**, 503–507 (2017).
38. Owen, S. F., Liu, M. H. & Kreitzer, A. C. Thermal constraints on in vivo optogenetic manipulations. *Nat. Neurosci.* **22**, 1061–1065 (2019).
39. Beier, K. T. et al. Circuit architecture of VTA dopamine neurons revealed by systematic input-output mapping. *Cell* **162**, 622–634 (2015).
40. Zheng, Z. W. et al. Hypothalamus-habenula potentiation encodes chronic stress experience and drives depression onset. *Neuron* **110**, 1400–1415.e1406 (2022).
41. Xie, Z. Y. et al. Mechanically evoked defensive attack is controlled by GABAergic neurons in the anterior hypothalamic nucleus. *Nat. Neurosci.* **25**, 72–85 (2022).
42. Wang, M. et al. Lateral septum adenosine A(2A) receptors control stress-induced depressive-like behaviors via signaling to the hypothalamus and habenula. *Nat. Commun.* **14**, 1880 (2023).
43. Stanić, D., Mulder, J., Watanabe, M. & Hökfelt, T. Characterization of NPY Y2 receptor protein expression in the mouse brain. II. Coexistence with NPY, the Y1 receptor, and other neurotransmitter-related molecules. *J. Comp. Neurol.* **519**, 1219–1257 (2011).
44. Stanić, D. et al. Characterization of neuropeptide Y2 receptor protein expression in the mouse brain. I. Distribution in cell bodies and nerve terminals. *J. Comp. Neurol.* **499**, 357–390 (2006).
45. Kopp, J. et al. Expression of the neuropeptide Y Y1 receptor in the CNS of rat and of wild-type and Y1 receptor knock-out mice. Focus on immunohistochemical localization. *Neuroscience* **111**, 443–532 (2002).
46. Seo, J. S. et al. Cellular and molecular basis for stress-induced depression. *Mol. Psychiatry* **22**, 1440–1447 (2017).

47. George, D. T., Ameli, R. & Koob, G. F. Periaqueductal gray sheds light on dark areas of psychopathology. *Trends Neurosci.* **42**, 349–360 (2019).
48. Yuan, Y. et al. Reward inhibits paraventricular CRH neurons to relieve stress. *Curr. Biol.* **29**, 1243–1251.e1244 (2019).
49. Bacchi, F. et al. Anxiolytic-like effect of the selective neuropeptide Y Y2 receptor antagonist BIIE0246 in the elevated plus-maze. *Peptides* **27**, 3202–3207 (2006).
50. Kask, A., Rägo, L. & Harro, J. Anxiolytic-like effect of neuropeptide Y (NPY) and NPY13-36 microinjected into vicinity of locus coeruleus in rats. *Brain Res.* **788**, 345–348 (1998).
51. Azevedo E. P., et al. A limbic circuit selectively links active escape to food suppression. *Elife* **9**, (2020).
52. Wu, Y. et al. The anterior insular cortex unilaterally controls feeding in response to aversive visceral stimuli in mice. *Nat. Commun.* **11**, 640 (2020).
53. Zhang, J., Chen, D., Sweeney, P. & Yang, Y. An excitatory ventromedial hypothalamus to paraventricular thalamus circuit that suppresses food intake. *Nat. Commun.* **11**, 6326 (2020).
54. Wang, D. et al. Lateral hypothalamus orexinergic inputs to lateral habenula modulate maladaptation after social defeat stress. *Neurobiol. Stress* **14**, 100298 (2021).
55. Owens-French, J. et al. Lateral hypothalamic galanin neurons are activated by stress and blunt anxiety-like behavior in mice. *Behav. Brain Res.* **423**, 113773 (2022).
56. Peyron, C. et al. Neurons containing hypocretin (orexin) project to multiple neuronal systems. *J. Neurosci.* **18**, 9996–10015 (1998).
57. Bonnavion, P., Jackson, A. C., Carter, M. E. & de Lecea, L. Antagonistic interplay between hypocretin and leptin in the lateral hypothalamus regulates stress responses. *Nat. Commun.* **6**, 6266 (2015).
58. Mercer, R. E., Chee, M. J. & Colmers, W. F. The role of NPY in hypothalamic mediated food intake. *Front. Neuroendocrinol* **32**, 398–415 (2011).
59. Zhu, C. J. et al. Profound and redundant functions of arcuate neurons in obesity development. *Nat. Metab.* **2**, 763–774 (2020).
60. Betley, J. N. et al. Neurons for hunger and thirst transmit a negative-valence teaching signal. *Nature* **521**, 180–185 (2015).
61. Comeras, L. B., Herzog, H. & Tasan, R. O. Neuropeptides at the crossroad of fear and hunger: a special focus on neuropeptide Y. *Ann. N.Y. Acad. Sci.* **1455**, 59–80 (2019).
62. Forbes, S., Herzog, H. & Cox, H. M. A role for neuropeptide Y in the gender-specific gastrointestinal, corticosterone and feeding responses to stress. *Br. J. Pharmacol.* **166**, 2307–2316 (2012).
63. Nectow, A. R. et al. Identification of a brainstem circuit controlling feeding. *Cell* **170**, 429–442.e411 (2017).
64. Verma, R., Balhara, Y. P. & Gupta, C. S. Gender differences in stress response: role of developmental and biological determinants. *Ind. Psychiatry J.* **20**, 4–10 (2011).
65. Claes, M., De Groef, L. & Moons, L. The DREADDful hurdles and opportunities of the chronic chemogenetic toolbox. *Cells* **11**, 1110 (2022).
66. Zhao, Z. et al. A central catecholaminergic circuit controls blood glucose levels during stress. *Neuron* **95**, 138–152.e135 (2017).
67. Mimee, A., Kuksis, M. & Ferguson, A. V. α-MSH exerts direct postsynaptic excitatory effects on NTS neurons and enhances GABAergic signaling in the NTS. *Neuroscience* **262**, 70–82 (2014).
68. Liu, Z. X. et al. Dorsal raphe neurons signal reward through 5-HT and glutamate. *Neuron* **81**, 1360–1374 (2014).
69. Li, Y. et al. Serotonin neurons in the dorsal raphe nucleus encode reward signals. *Nat. Commun.* **7**, 10503 (2016).

Acknowledgements

This work is supported by grants from the STI2030-Major Projects (2021ZD0203900 to C.Z.), the National Key R&D Program of China (2019YFA0801900 to T.L.), the National Natural Science Foundation of China (32271063, 31822026, 31500860 to C.Z.), Research Funds of Center for Advanced Interdisciplinary Science and Biomedicine of IHM (QYPY20220018 to C.Z.), the National Natural Science Foundation of China (92357304, 92249302 to T.L.), the Shanghai Municipal Science and Technology Major Project, International Human Phenome Project II (2023SHZDZX02 to T.L.), Faculty Resources Project of College of Life Sciences, Inner Mongolia University (2022-102 to T.L.), Shanghai Frontiers Science Research Base of Exercise and Metabolic Health, the National Natural Science Foundation of China (32171144 to Z.Z.) and Shanghai Pujiang Program (22PJD007 to Z.Z.).

Author contributions

T.L. and C.Z. conceived the study. Y.Z. and C.Z. wrote the manuscript. Y.Z., J.S., F.X., Z.L., M.C., and M.C. conducted the experiments. F.Y. and L.W. built behavioral test apparatuses and the fiber photometry system. H.H., P.W. and Z.Z. provided intellectual expertise, assisted in interpreting the experimental findings and contributed to the manuscript revisions.

Competing interests

The authors declare no competing interests.

Additional information

Supplementary information The online version contains supplementary material available at https://doi.org/10.1038/s41467-024-51956-9.

Correspondence and requests for materials should be addressed to Zhi Zhang, Cheng Zhan or Tiemin Liu.

Peer review information *Nature Communications* thanks the anonymous reviewers for their contribution to the peer review of this work. A peer review file is available.

Reprints and permissions information is available at http://www.nature.com/reprints

Publisher's note Springer Nature remains neutral with regard to jurisdictional claims in published maps and institutional affiliations.

Open Access This article is licensed under a Creative Commons Attribution-NonCommercial-NoDerivatives 4.0 International License, which permits any non-commercial use, sharing, distribution and reproduction in any medium or format, as long as you give appropriate credit to the original author(s) and the source, provide a link to the Creative Commons licence, and indicate if you modified the licensed material. You do not have permission under this licence to share adapted material derived from this article or parts of it. The images or other third party material in this article are included in the article's Creative Commons licence, unless indicated otherwise in a credit line to the material. If material is not included in the article's Creative Commons licence and your intended use is not permitted by statutory regulation or exceeds the permitted use, you will need to obtain permission directly from the copyright holder. To view a copy of this licence, visit http://creativecommons.org/licenses/by-nc-nd/4.0/.

© The Author(s) 2024